Volume 54
Number 7
7 April 2025
Pages 3235–3600

Chem Soc Rev

Chemical Society Reviews

rsc.li/chem-soc-rev

ISSN 0306-0012

ROYAL SOCIETY OF CHEMISTRY

REVIEW ARTICLE

Hiroshi Yukawa, Hidetoshi Kono, Yoshinobu Baba *et al.*
Quantum life science: biological nano quantum sensors, quantum technology-based hyperpolarized MRI/NMR, quantum biology, and quantum biotechnology

Chem Soc Rev

REVIEW ARTICLE

View Article Online
View Journal | View Issue

Check for updates

Cite this: *Chem. Soc. Rev.*, 2025, **54**, 3293

Quantum life science: biological nano quantum sensors, quantum technology-based hyperpolarized MRI/NMR, quantum biology, and quantum biotechnology

Hiroshi Yukawa, * Hidetoshi Kono, * Hitoshi Ishiwata, Ryuji Igarashi, Yoichi Takakusagi, Shigeki Arai, Yu Hirano, Tetsuya Suhara and Yoshinobu Baba *

The emerging field of quantum life science combines principles from quantum physics and biology to study fundamental life processes at the molecular level. Quantum mechanics, which describes the properties of small particles, can help explain how quantum phenomena such as tunnelling, superposition, and entanglement may play a role in biological systems. However, capturing these effects in living systems is a formidable challenge, as it involves dealing with dissipation and decoherence caused by the surrounding environment. We overview the current status of the quantum life sciences from technologies and topics in quantum biology. Technologies such as biological nano quantum sensors, quantum technology-based hyperpolarized MRI/NMR, high-speed 2D electronic spectrometers, and computer simulations are being developed to address these challenges. These interdisciplinary fields have the potential to revolutionize our understanding of living organisms and lead to advancements in genetics, molecular biology, medicine, and bioengineering.

Received 29th June 2024

DOI: 10.1039/d4cs00650j

rsc.li/chem-soc-rev

Open Access Article. Published on 28 Januarie 2025. Downloaded on 2026-01-31 2:57:56 nm..
This article is licensed under a Creative Commons Attribution-NonCommercial 3.0 Unported Licence.

1. Introduction

Quantum life science is an emerging field that combines principles from quantum physics and biology to study and understand various fundamental life processes such as

Institute for Quantum Life Science, National Institutes for Quantum Science and Technology (QST), Anagawa 4-9-1, Inage-ku, Chiba 263-8555, Japan. E-mail: yukawa.hiroshi@qst.go.jp, kono.hidetoshi@qst.go.jp, baba.yoshinobu@qst.go.jp

Hiroshi Yukawa

Dr Hiroshi Yukawa is a Project Director, Institute for Quantum Life Science in National Institutes for Quantum Science and Technology, Japan, and a Designated Professor, Institute of Nano-Life-Systems, Institutes of Innovation for Future Society, Nagoya University. He received his PhD in Medical Science from Nagoya University in 2010 under the supervision of Professor M. Hamaguchi, and received his PhD in Engineering from Tokyo University in 2011 under the supervision of Professor K. Araki. His current research focus is the application of quantum nano sensors to advanced medical sciences such as regenerative medicine, cancer medicine, and cranial nerves medicine.

Hidetoshi Kono

Dr Hidetoshi Kono earned his PhD from The University of Tokyo. After postdoctoral work at RIKEN's Tsukuba Life Science Center and the University of Pennsylvania, he joined the Japan Atomic Energy Agency. In 2007, he established a research group studying protein–DNA interactions through molecular modeling. Now Deputy Director General at the Institute for Quantum Life Science, National Institutes for Quantum Science and Technology, he investigates gene regulation mechanisms through molecular modeling, simulation, and single-molecule measurements using optical tweezers.

Open Access Article. Published on 28 Januarie 2025. Downloaded on 2026-01-31 2:57:56 nm.
This article is licensed under a Creative Commons Attribution-NonCommercial 3.0 Unported Licence.

photosynthesis, respiration, and magnetoreception at the molecular level. It explores how quantum phenomena, such as the tunnelling effect, quantum superposition, and quantum entanglement, may play a role in biological processes and systems. However, capturing such quantum effects is still challenging because the surrounding environment quickly causes dissipation and decoherence of the quantum system in warm and wet living systems. Quantum mechanics is the fundamental theory that can describe the properties of small particles such as electrons, atoms, and even molecules. All living systems are made up of molecules, and fundamentally, all molecules are described by quantum mechanics. However, there is a remarkable size and time scale gap between the system in which quantum mechanics operates and the living system. The technologies that will help solve these problems include biological nano quantum sensors, quantum technology-based hyperpolarized MRI/NMR, and molecular dynamics simulation.

Quantum sensors are quantum devices that respond to external stimuli. Quantum sensors possess three characteristics: (1) discrete energy levels; (2) initialization, coherent manipulation, and readout; and (3) interaction with physical quantities. In particular, the nitrogen-vacancy-center (NV center), a fluorescent lattice defect that exists only slightly in diamond crystals, is attracting attention as a biological nano quantum sensor that functions at room temperature and pressure because of its high affinity to cells and living organisms. Quantum technology-based hyperpolarized MRI/NMR is the only method that employs quantum phenomena based on nuclear spin manipulation as the detection principle to detect the relaxation process among the various available medical diagnostic imaging techniques. This signal is expected to make it possible to monitor molecular and structural changes in many metabolites derived from cells and living bodies using

Hitoshi Ishiwata

Dr Hitoshi Ishiwata currently holds the position of Chief Researcher at the Institute for Quantum Life Science (iQLS), a part of the National Institutes for Quantum Science and Technology (QST). He completed his PhD at Stanford University in 2016, where he specialized in the use of diamondoids for photonics application and diamond growth. Following his doctoral studies, he focused on the fabrication of quantum sensors and the development of quantum measurement systems designed for the label-free detection of molecules within nanoscale detection volume. His expertise spans the fields of quantum sensor fabrication and quantum measurements of biological molecules.

Ryuji Igarashi

Dr Ryuji Igarashi is the Team Leader at the Institute for Quantum Life Science, part of the National Institutes for Quantum Science and Technology. He earned his PhD in Engineering from Kyoto University. Specializing in nanobioscience based on quantum sensing, Dr Igarashi has pioneered various measurement techniques using nanodiamond NV centers. He has developed selective fluorescence imaging, pH nanosensors, and three-dimensional rotational measurements. Furthermore, Dr Igarashi has been at the forefront of applying these techniques to biometric measurements, leading to notable advancements in the field.

Yoichi Takakusagi

Dr Yoichi Takakusagi is currently the Team Leader at the National Institutes for Quantum Science and Technology (QST), and a visiting Professor in Chiba University. He received his PhD in Pharmaceutical Science with honors from Tokyo University of Science in 2006. He joined the group of Dr Murali K. Cherukuri at NCI/NIH from 2011 to 2014. He belonged to Kyushu University (2014) and The University of Tokyo (2015) as a research fellow in the JST/CREST hyperpolarized NMR/MRI research project (Prof. Sando's team). His research interest lies in the development and application of theranostics.

Shigeki Arai

Dr Shigeki Arai received his PhD in 1999 from Gunma University, Japan. After postdoctoral research (1999–2004) in Neutron Science Research Center at Japan Atomic Energy Research Institute, he took up a position in Quantum Beam Science Directorate at Japan Atomic Energy Agency (2004–2016). In 2016, he moved to National Institutes for Quantum Science and Technology in Japan as a senior principal researcher. His research interests include quantum biology, biophysics, and quantum beam science.

 This journal is © The Royal Society of Chemistry 2025

Open Access Article. Published on 28 Januarie 2025. Downloaded on 2026-01-31 2:57:56 nm.
This article is licensed under a Creative Commons Attribution-NonCommercial 3.0 Unported Licence.

the nuclear frequency of the NMR-positive nuclei as the chemical shift alteration at arbitrary magnetic field strength. In addition, practically and effectively, molecular dynamics simulation with the atomic model based on biomolecules' 3D structures has contributed a lot to understanding how they function to achieve biological processes based on classical molecular mechanics. However, classical molecular mechanics cannot treat quantum effects because they employ empirical force fields that define fixed covalent bond topologies and typically fixed atomic charges. An open quantum systems (OQS) approach was recently applied to study proton tunnelling in the base pair of DNA.[1] The OQS suggests that the proton transfer rate between the G–C base pair is several orders of magnitude larger than that calculated d by the classical mechanics, indicating DNA base mutation is more likely to occur in the living system.

These interdisciplinary fields in quantum life sciences have the strong potential to revolutionize our understanding of living organisms and will lead to advancements in genetics, molecular biology, medicine, and bioengineering (Fig. 1).

Yu Hirano

Dr Yu Hirano received his PhD in 2007 from Graduate School of Science, Kyoto University, Japan. After postdoctoral research in Ibaraki University (2007–2009), in Kyoto University (2009–2013) and in Japan Atomic Energy Agency (2013–2016), he moved to National Institutes for Quantum Science and Technology as a senior researcher. His research interests include reaction mechanism catalyzed by redox proteins with high-resolution structural information.

2. Biological nano quantum sensors

2.1. Quantum sensing and quantum systems

Quantum sensing harnesses quantum properties, including coherence, interference, and entanglement, to measure physical parameters with unparalleled precision and sensitivity.[2–5] These quantum sensors often outperform their classical counterparts, enhancing accuracy across multiple applications. Traditionally, quantum sensors are built using superconductive devices,[6] OPM,[7] and trapped ions.[8] However, these systems come with challenges. They demand extreme conditions, such as ultra-low temperatures and near-perfect vacuums, making them less feasible for biological measurements. Solid state spins such as NV centers in diamonds have emerged as brilliant solutions for applying quantum sensing to biological applications.[9,10] Wide bandgap materials are perfect hosts for these spin states, producing isolated energy levels within solid-state crystals. Consequently, this results in electron spin states with coherence times spanning several microseconds, which are manipulable even at room temperature. The creation of new color centers has gained significant traction over the past decade, with researchers identifying over 500 such centers in materials like diamond,[11] silicon carbide (SiC),[12] hexagonal boron nitride (h-BN),[13] aluminum nitride (AlN)[14] and gallium nitride (GaN).[15] Owing to its low spin–orbit coupling and the optimal photo cycle for spin state initialization and readout, the NV center in the diamond exhibits an extended coherence time and pronounced contrast. Moreover, a notable advantage of diamond NV center-based quantum sensors is their photostability[16] and single-spin sensitivity.[17] Conventional biological sensors, such as those using fluorescent dyes or proteins, require ensembles of molecules to achieve a reliable signal. This, in turn, demands larger measurement volumes, often in the micrometer range, due to optical instability. In contrast, NV centers in diamonds exhibit exceptional photostability and can function as highly sensitive sensors, even as individual lattice defects within molecular-sized particles.[18] This enables fluorescent nanodiamonds to serve as

Tetsuya Suhara

Dr Tetsuya Suhara is a psychiatrist and received PhD degree in 1991 from Jikei University School of medicine. He is now a Managing Director of Quantum Life and Medical Science Directorate, National Institutes for Quantum Science and Technology (QST). He has been using positron emission tomography (PET) to investigate the mechanism of neuropsychiatric disorders. Then he participated in the establishment of Quantum Life Science field in QST as a Deputy Director General of Institute for Quantum Life Science. He is author or co-author of 400 research publications.

Yoshinobu Baba

Dr Yoshinobu Baba received PhD degree from Kyushu University. He is now a Director General of Institute for Quantum Life Science, QST and a Professor of Nagoya University. He has been admitted as a Fellow of the Royal Society of Chemistry and received over 100 awards, prizes, and Medal. He is the author or co-author of 1160 publications and also an inventor of over 131 patents. He has delivered more than 1112 plenary and invited lectures. His work has been cited on 522 occasions by newspapers and television.

Open Access Article. Published on 28 Januarie 2025. Downloaded on 2026-01-31 2:57:56 nm..
This article is licensed under a Creative Commons Attribution-NonCommercial 3.0 Unported Licence.

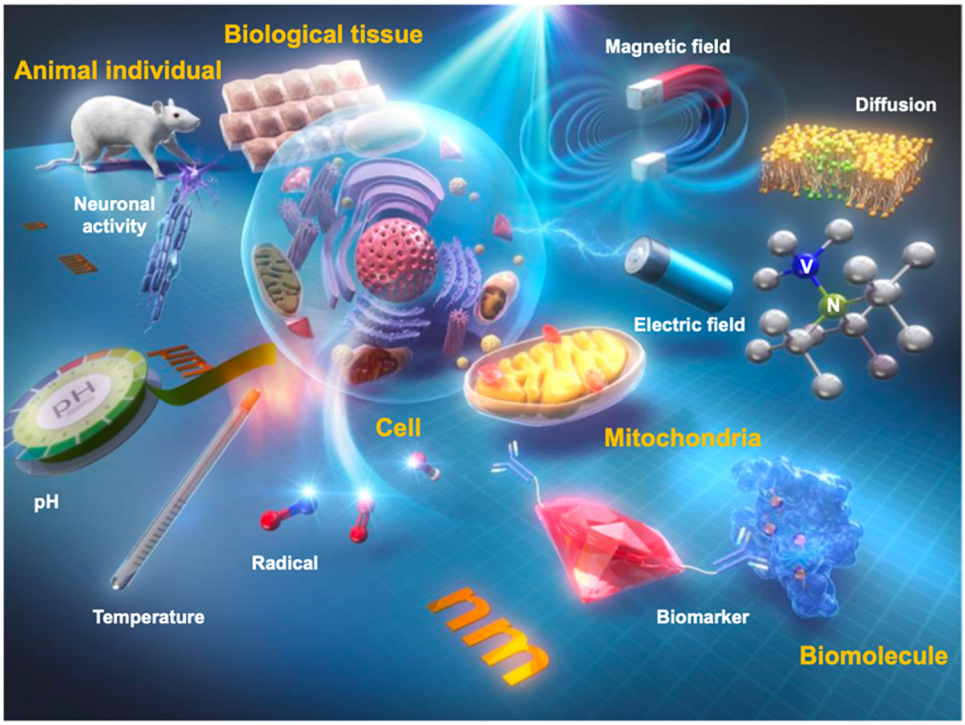

Fig. 1 Conceptual diagram of biological nano quantum sensors. Realization of nanodiamond quantum sensors to measure physicochemical parameters such as temperature, pH, magnetic field, and electric field in cells and living organisms.

nanoscale sensors, allowing precise measurements of physical and chemical parameters in biological microenvironments like mitochondria[19] or membrane proteins.[20] Consequently, it has been increasingly recognized as a color center for biological application, finding applications in areas such as *in vivo* thermometry[21] and in-cell organelle measurements.[19] The NV center's precise positioning is pivotal for advancing biological applications. Advancements like single-protein NMR (Fig. 2a–c)[22] and single-molecule ESR (Fig. 2d–f)[23] owe their success to accurately positioning an NV center nanometers away from the target spin. Upon integration into biological systems, quantum sensors can detect a range of physical attributes – magnetic[24] and electric fields,[25] temperature,[26] pressure,[27] and molecular diffusion[28,29] with a groundbreaking sensitivity.

2.2. Sensitivity of quantum sensors

The sensitivity of a quantum sensor is fundamentally governed by spin projection noise. The sensitivity of the NV center in diamond is distinctively characterized by its optical readout.[31] This is quantitatively represented by the shot-noise limited sensitivity, $\delta B(\tau) = \frac{1}{\gamma C\sqrt{NT}}$. Here T represents the coherent duration of a singular measurement. γ is the linear rate at which the spin state population changes concerning the unit target signal. N signifies the number of quantum sensors deployed in the measurement. The choice of measurement protocol directly influences the value of T. For instance, T is derived from T_{2^*} when employing the Ramsey measurement, whereas the Hahn-echo measurement necessitates deriving T from T_2. Coherence enhancement achieved predominantly by mitigating spin noise sources like surrounding electrons and nuclear spins can augment the value of T. The parameter C is contingent upon the NV center's orientation within the diamond crystal lattice and its charge state. Conversely, N is influenced by the density of the diamond's NV centers and the optical excitation volume. The latter can be modulated by varying the optical excitation techniques, transitioning from, for example, confocal to bulk excitation methods. Subsequent sections will elucidate processes tailored to augment the intrinsic quality of the host crystal, methodologies for producing NV centers in diamond, and protocols for diamond surface treatments, all aimed at optimizing the parameters mentioned above.

Quantitative analysis of the sensitivity of an NV center in diamond was achieved by applying an AC magnetic field synchronized with quantum manipulation pulses. The sensitivity was quantified by measuring the amplitude of the signal as a function of measurement time, and analyzing the resulting Allan deviation, as illustrated in Fig. 2g. An Allan deviation corresponding to a sensitivity of 0.9 $\mathrm{pT}/\sqrt{\mathrm{Hz}}$ at a frequency of 20 kHz was obtained.

2.3. Host crystal

The quality, inherent, and purity of the host material are pivotal in enhancing the coherence time of the NV center. Historically, the synthesis of diamond crystals has been challenging due to the greater stability of sp^3-bonded carbon compared to sp^2-bonded carbon at both atmospheric and lower temperatures. Consequently, it is difficult to produce diamond without the

 This journal is © The Royal Society of Chemistry 2025

Open Access Article. Published on 28 Januarie 2025. Downloaded on 2026-01-31 2:57:56 nm..
This article is licensed under a Creative Commons Attribution-NonCommercial 3.0 Unported Licence.

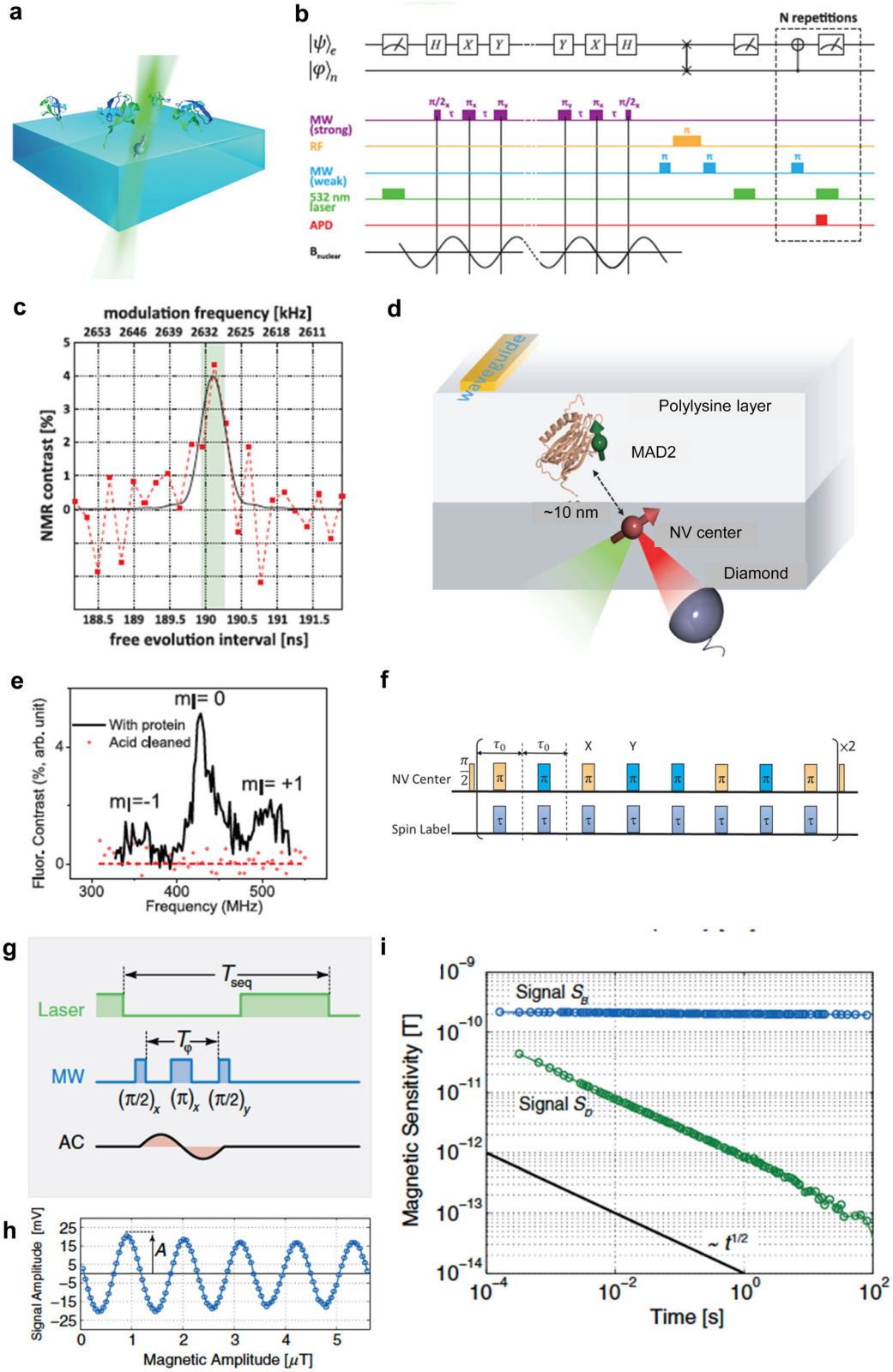

Fig. 2 Measurement of a single NV center. (a) Schematic depicting the experimental setup of ubiquitin proteins covalently tethered to the diamond's surface above a single NV center. (b) Pulse sequence for quantum sensing for detection of nuclear spin from single protein. (c) NMR spectra of ^{13}C originating from a single ubiquitin protein. (d) Schematic depicting the experimental setup of MAD2 proteins labeled with nitroxide spin labels above a single NV center. (e) Pulse sequence for quantum sensing for detection of electron spin from a single protein. (f) Single spin ESR spectra under ambient conditions. (g) AC magnetic-field measurement scheme with pulsed sensor readout (h). Magnetic measurement of the test field with varying field amplitude retrieving sensor response A (i). Scaling of magnetic sensitivity (standard deviation over time) of signal SB (blue line) and SD (green line). The slope of the black line again indicates the aspired scaling behavior with $\sqrt{t}$. Reproduced from ref. 22, 23 and 30 with permission from AAAS and APS.

Open Access Article. Published on 28 Januarie 2025. Downloaded on 2026-01-31 2:57:56 nm.
This article is licensed under a Creative Commons Attribution-NonCommercial 3.0 Unported Licence.

concurrent formation of sp^2-bonded carbon, such as graphite. This distinction was notably illustrated in the Bachmann diagram during the early phases of diamond research.[32] Industrial synthetic single-crystal diamonds are primarily synthesized using the high-pressure-high-temperature (HPHT) method. While diamonds produced *via* HPHT exhibit low strain, this technique grapples with issues related to precise impurity concentration control.[33] Furthermore, managing the thickness and exact positioning of the quantum sensor remains a challenge with HPHT. An alternative approach, plasma-enhanced chemical vapor deposition (CVD), facilitates the homoepitaxial growth of diamond on HPHT substrates using CH_4 as a carbon source. H_2 serves as a carrier gas, producing a plasma that preferentially etches sp^2 carbon formed during growth, ensuring the retention of sp^3 carbon for premium diamond synthesis. Commercially, diamonds produced through CVD growth are available with nitrogen and boron concentrations of less than one part per billion.[34] Further advancements include the isotopic purification of diamond crystals. Here, the naturally occurring 1% of ^{13}C is refined to levels approaching 99.999% using highly isotopically purified gases.[35] Employing high-quality diamond substrates, especially those with extreme isotopic purity, has resulted in record-setting coherence times of $\sim$1 ms for single NV centers in diamond (Fig. 3a–c).[36]

2.4. Fabrication of NV center

The fabrication of the NV center in diamond requires the precise introduction of nitrogen atoms and adjacent vacancies. This process is particularly challenging due to the extreme hardness of diamond, which complicates the insertion of impurities in close proximity[40] to vacancies and necessitates specialized fabrication techniques. Conventional methods employ ion implantation to introduce nitrogen, electron irradiation to induce vacancies, and thermal annealing to promote the diffusion and consequent formation of the NV center within the diamond lattice.[41] Through ion implantation, one can exert meticulous control over the spatial positioning of the introduced nitrogen, choose between the ^{14}N or ^{15}N isotopes, and regulate the concentration of NV centers formed in the host crystal.[42] Leveraging this technique, a singular NV center has been successfully positioned as close as 10 nm from the diamond's surface,[43] proving invaluable for single protein and single electron spin detection applications. The distinctiveness of the incorporated nitrogen isotope further aids in the unequivocal identification of the introduced species.[23] To achieve precise spatial control over NV center location, integration with nanofabricated masks,[44] focused ion beams,[45] or nanometric apertures in AFM tips[46] has been pursued. However, the exact depth control remains constrained to an approximation of 10 nm, a limitation arising from ion scattering and channeling phenomena.[47] An alternative technique, laser writing, has demonstrated potential in generating vacancies and enabling three-dimensional localization of NV centers.[48] Nevertheless, its in-plane accuracy remains tethered to the average inter-nitrogen spacing due to inherent challenges with vacancy diffusion.

CVD growth is a prominent technique for precisely controlling the position, isotope, and alignment of the NV center within the diamond. Given that the nitrogen-to-carbon ratio can be adjusted by varying the gas ratio of nitrogen (N_2) to methane (CH_4), CVD offers unparalleled control over the NV center's density and nitrogen incorporation into the diamond matrix. The most substantial NV center densities within the diamond have been achieved by combining CVD growth, which introduces a high nitrogen concentration into the diamond, with electron irradiation at either the MeV range or 200 keV using an electron source from TEM.[49,50] A lower acceleration voltage introduces vacancies more gently, resulting in enhanced coherence times and favorable NV center generation ratios. Recent innovations have facilitated the creation of high-density NV centers in diamonds, enabling the observation of spin interactions between adjacent NV centers. Furthermore, controlling the timing of gas introduction during CVD growth affords precision over the thickness and location of the resulting NV center. Through delta doping of nitrogen gas, CVD growth can confine the formation of an NV center within a tight 1–2 nm region.[51]

In the process where electron irradiation is paired with nitrogen implantation, the formation of the NV center in a diamond generally assumes a random orientation among the four possible [111] directions ([111], [$\bar{1}\bar{1}$1], [1$\bar{1}\bar{1}$], [$\bar{1}$1$\bar{1}$]). To date, CVD growth remains the sole method allowing for the deliberate alignment of the NV center in the diamond crystal towards one of these four directions, enhancing the NV center's contrast to an optimal photo-cycle limit of approximately 30%. Alignment of the NV center within the diamond lattice *via* step-flow growth using a reduced methane concentration has been experimentally demonstrated by T. Fukui *et al.*,[52] with corroborating theoretical calculations by T. Miyazaki *et al.*[53] Subsequent research has pursued objectives like achieving a high-density ensemble of perfectly aligned NV centers,[54] precisely aligned shallow NV centers suitable for nanoscale NMR measurements,[55] and a 100 μm-thick diamond crystal tailored for high sensitivity applications.[56] Incorporating *tert*-butylphosphine as a gaseous precursor during CVD growth has been explored to enhance the coherence time of these perfectly aligned NV centers.[57] Furthermore, phosphorous doping *via* CVD growth has been employed to optimize the charge state of the NV center in diamonds, setting new benchmarks for the T_2 and T_{2^*} values observed in individual NV centers.[58]

2.5. Nanodiamond

Nanodiamonds have been fabricated through many approaches, encompassing the detonation technique,[59] high-pressure high-temperature (HPHT) synthesis,[60] laser ultrasound cavitation,[61] ablation,[62] and microfabrication.[63] The key metrics of interest for NV centers in nanodiamonds encompass the NV center's stability (attributed to charge state management), the quantity of NV centers, and the coherence time of the NV center within the diamond. This review delineates the distinctions between nanodiamonds synthesized *via* the detonation technique and HPHT synthesis, as these methods dominate commercial nanodiamond production.

Detonation nanodiamonds (DNDs) derive from the detonation process. Specifically, the explosion of trinitrotoluene (TNT) and hexogen (RDX) blend within a confined metal chamber,

 This journal is © The Royal Society of Chemistry 2025

Open Access Article. Published on 28 Januarie 2025. Downloaded on 2026-01-31 2:57:56 nm..
This article is licensed under a Creative Commons Attribution-NonCommercial 3.0 Unported Licence.

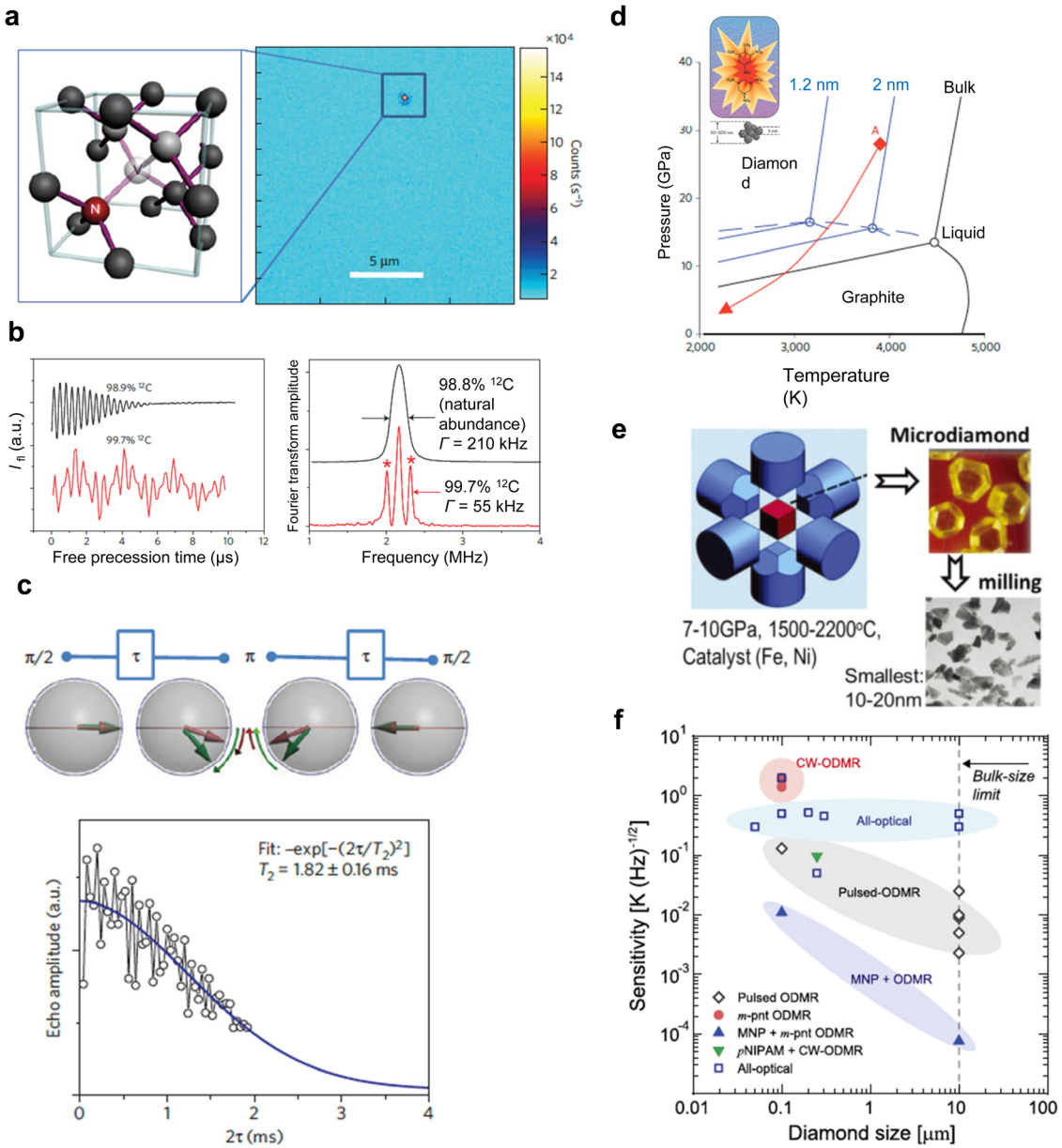

Fig. 3 Spin coherence time of single spins in isotopically engineered diamond. (a) Fluorescence microscopy image of high-purity CVD diamond containing single nitrogen-vacancy defects. (b) FID signal measured on a single nitrogen-vacancy electron spin for diamond with a natural abundance of ^{13}C isotope (black) and isotopically engineered crystal (red). And Fourier-transform spectra of FID signals. The satellites indicated by asterisks are related to the hyperfine interaction with the nitrogen and carbon nuclei. (c) Spin coherence time of single spins in isotopically engineered diamond measured using a two-pulse electron spin echo. (d) Detonation NDs produced by the detonation of carbon-containing explosives. The phase diagram shows that the most stable carbon phases for graphite and diamond are at low and high pressures, melting at temperatures above 4500 K. The phase diagrams for nanoscale carbon shows liquid phase at lower temperatures. In detonation, the pressure and temperature rise instantaneously, reaching the Jouguet point (point *A*), which falls within the region of liquid carbon clusters of 1–2 nm in size. As the temperature and pressure decrease along the red line, the growth of the diamond is replaced by the formation of graphite. (e) NDs produced by the HPHT methods. (f) Plots of temperature sensitivity *versus* diamond size Reproduced from ref. 36–39 with permission from Nature Portfolio, AIP Publishing and IOP Publishing Ltd.

leading to the high-pressure, high-temperature formation of 4–5 nm nanodiamonds (Fig. 3d and e).[37] The hallmark of this method is its consistent yield of uniformly sized 4–5 nm nanodiamonds. However, DNDs often manifest as polycrystalline or ultra-nanocrystalline diamonds, typified by a patchwork of minute crystalline domains interspersed with sp^2 carbon (such as graphite) grain boundaries. This results in elevated surface tension.[64] The nitrogen concentration (P1 center) in DNDs, at approximately 1000 ppm, markedly exceeds that of HPHT-derived nanodiamonds, which hover around 100 ppm. This trait appears to favor the generation of NV centers in DNDs relative to HPHT nanodiamonds.[65] Despite their high NV center content, DNDs are frequently sheathed in graphitic layers, necessitating rigorous cleaning protocols, such as acid

Open Access Article. Published on 28 Januarie 2025. Downloaded on 2026-01-31 2:57:56 nm.
This article is licensed under a Creative Commons Attribution-NonCommercial 3.0 Unported Licence.

treatments supplemented with sonication, to ensure stable emission of NV centers.[18,64–66]

Conversely, the predominant method for producing quantum sensing-applicable nanodiamonds entails milling HPHT micro-diamonds. Within the HPHT reactor, metal catalysts (like Fe, Ni, or Co) operate under extreme conditions to engender micro-diamonds infused with nitrogen (Fig. 3f).[38,67] Post-fabrication, NV centers within these micro-diamonds are realized through electron irradiation, annealing, mechanical milling, and oxidation (a regimen designed to purge surface contaminants).[68] Despite its prevalence in commercial nanodiamond production, this procedure has flaws. The mechanical milling phase tends to diminish the count of NV centers in the resultant nanodiamonds. Therefore, innovations that miniaturize micro-diamonds without compromising NV center quantities are actively sought. Recent research spotlighting HPHT diamond synthesis using molecular diamonds, termed "diamondoids" (*e.g.*, adamantane), has renewed the field.[69] The introduction of new catalysts has enabled reduced pressure and temperature conditions for HPHT synthesis stemming from adamantane.[70] However, this method faces a significant challenge: adamantane, a diminutive diamond structure with a mere ten carbon atoms, is highly susceptible to disintegration. Any reaction undermining its structure will obliterate this diamond configuration, making reactions seeded by such a molecular diamond inherently unstable. Exploring larger molecular diamonds, like pentamantane, might pave the way for innovative nanodiamond production methodologies.[71]

The sensitivity of nanodiamonds, as discussed in Section 2.2, is influenced by several factors including longer coherence times, larger contrast, and a higher number of NV centers, which collectively enhance the measurement sensitivity of nanodiamonds. However, substantial variations exist in the actual values of these parameters, even when identical fabrication methods are used. Fig. 3f illustrates the dependence of sensitivity on the size of the nanodiamonds.[39] Despite the inherent limitations in the characteristics of nanodiamonds, various measurement techniques have been developed to enhance sensitivity. The highest sensitivity has been achieved by integrating Magnetic Nano Particles (MNP) with nanodiamonds, a method that now rivals the sensitivity achieved by the MNP + ODMR methods due to recent advancements in nanodiamond fabrication.[72]

2.6. Diamond surface

Both single NV centers in diamond films and nanodiamonds offer material interfaces beneficial for biological applications. This is underscored by extensive research into the alteration of surface conductivity due to changes in surface termination.[73] The charge state of the NV center that determines the stability of emission, contrast, and location of the NV center from the target of detection is controlled by the surface termination of diamonds. For single NV centers in diamond films, their precise localization relative to the diamond surface could be well defined by quantum measurement. Extensive studies have been performed to elucidate the effect of surface termination on location,[43] contrast,[74] and coherence[75] of the NV center. Correlating quantum measurements with surface analysis *via* NEXAFS has deepened our understanding of diverse oxidation methodologies for diamond surfaces. Optimal conditions for a single NV center on a diamond film surface have been identified: air oxidation at 450 °C, which results in an optimized coherence time of 100 μs for centers located within 10 nm from the diamond surface.[76] In contrast, nanodiamond surfaces often contend with contaminants like metal impurities, soots, and sp^2 carbons during fabrication. These are typically removed through oxidizing acids or air oxidation, leading to carbonyl and carboxyl groups forming on the nanodiamonds.[77–79] Much research has been dedicated to the surface functionalization of diamond films and nanodiamonds, specifically for the conjugation of molecules and proteins, offering a biological interface tailored for diverse applications.[80–83] The prevailing challenge lies in precisely positioning the NV center within 5 nm from the surface, all while maintaining extended coherence times. Moreover, there's a need to accurately position biological targets on nanodiamonds or diamond films for prospective applications.

2.7. Sensing by NV center

Nitrogen-vacancy centers (NV centers) are fluorescent lattice defects with impurity nitrogen and vacancies next to each other. Negatively charged NV centers have a stable triplet electron pair at room temperature. They are well known to emit strong near-infrared fluorescence with a quantum yield >0.7 upon photoexcitation at around 520–540 nm.[84] Hereafter, NV centers with a negative charge will be called "NV centers."

An NV center functions as a quantum sensor by acquiring various physical and chemical information from the microenvironment as perturbations to the state of triplet electron spins. The energy levels of the triplet electron spins are approximated by the following spin Hamiltonian:

$$\begin{aligned} H &= \left(hD + d_{\parallel}\Pi_z\right)\left[S_z^2 - \frac{1}{3}S(S+1)\right] \\ &\quad - d_{\perp}\left[\Pi_x\left(S_x^2 - S_y^2\right) + \Pi_y\left(S_xS_y - S_yS_x\right)\right] \\ &\quad + \mu_B g_e\left(\vec{S}\cdot\vec{B}\right) \end{aligned} \tag{1}$$

where $\vec{S}$ is the spin operator of the electron spin, D is the zero-field splitting width based on the spin–spin interaction, $d_{\parallel}$ and $d_{\perp}$ are the parallel and perpendicular components of the electric dipole moment, $\vec{\Pi}$ is the electric field, μ_B is the Bohr magneton, g_e is the Landé g-factor for the NV center electron, $\vec{B}$ is the magnetic field. Thus, it can be seen that the energy levels of the NV center change under various perturbations, such as electric and magnetic fields or thermal expansion of the crystal lattice, which can affect the spin–spin interaction.

The electron spin state of the NV center can be determined based on the fluorescence intensity because the spin magnetic quantum number of the triplet electron spin is strictly conjugated to its electronic transition pathway in the NV center. Fig. 4a shows the paths of electronic and spin transitions of the electron spins. Almost all the occupied electrons in the $|0\rangle$ emit photons through vibrational relaxation of the normal fluorescence pathway. On the

 This journal is © The Royal Society of Chemistry 2025

Open Access Article. Published on 28 Januarie 2025. Downloaded on 2026-01-31 2:57:56 nm..
This article is licensed under a Creative Commons Attribution-NonCommercial 3.0 Unported Licence.

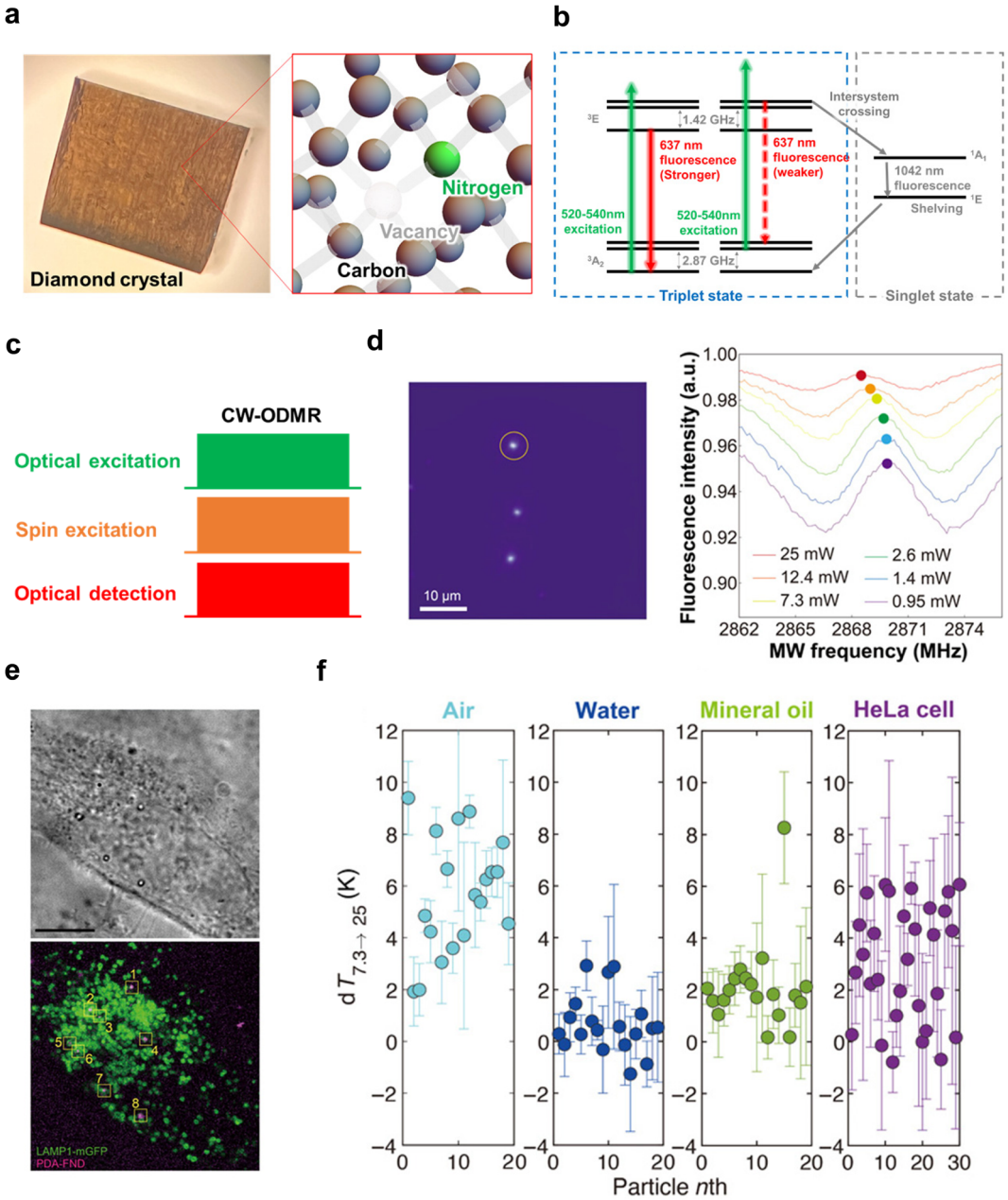

Fig. 4 Characteristics of the diamond NV center and measurement example using CW-ODMR. (a) Left: Photograph of a Type Ib diamond substrate after enrichment of NV centers through electron irradiation. Right: Schematic representation of the lattice defect structure of the NV center in diamond. (b) Energy level diagram of the NV center, illustrating various electron transition processes corresponding to different values of the spin magnetic quantum number, ms. (c) A typical pulse sequence of CW-ODMR. (d) Fluorescent image of thermogenic fluorescent nanodiamonds based on polydopamine surface coating. The ODMR frequency spectra detected from the NV center of the nanodiamond marked by the yellow circle in the image at different excitation laser powers are also shown. A temperature increase with rising laser power is observed as a low-frequency shift in ODMR. (e) Bright-field image (top) and fluorescence image (bottom) of HeLa cells overexpressing LAMP1-mGFP incubated for 4 hours with polydopamine-coated fluorescent nanodiamonds. (f) Thermal conductivity measurements in air, water, mineral oil, and HeLa cells. Circles with error bars represent the mean and standard deviation (SD) of changes in excitation power from 7.3 mW to 25 mW (denoted as dT7.3 → 25) measured for individual particles under different conditions. The numbers on the *x*-axis refer to the identifiers given to particles used in measurements for each medium.[87] Fig. 4d–f were reproduced from ref. 87 with permission from AAAS, copyright 2021.

other hand, about half of the electrons in the $|\pm1\rangle$ undergo vibrational relaxation through the intersystem crossing, in which they transit to and shelved in the singlet state and then return to the triplet state without emitting any fluorescence.[85] The lifetime of vibrational relaxation in the fluorescence pathway is about 10 ns, whereas the lifetime of vibrational relaxation *via* intersystem crossing is more than 10 times longer.[85,86] This means that the photoexcited electrons in the $|\pm1\rangle$ state cannot be ready for the next fluorescence cycle for a much longer time than those in the $|0\rangle$ state, emitting weaker fluorescence. Therefore, the spin

Open Access Article. Published on 28 Januarie 2025. Downloaded on 2026-01-31 2:57:56 nm.
This article is licensed under a Creative Commons Attribution-NonCommercial 3.0 Unported Licence.

population is determined based on the fluorescence intensity, and the magnetic resonance is measured by optical detection. This measurement, called optically detected magnetic resonance (ODMR), is the basis of quantum sensing using NV centers.

However, this mechanism cannot fully explain why NV centers can function as highly sensitive sensors. In fact, the triplet electron spin in the NV center has an energy level difference of only 2.87 GHz between $|0\rangle$ and $|\pm1\rangle$ at zero magnetic fields, and the Zeeman energy follows the electron magnetic rotation ratio of 2.8 MHz Gauss^{-1}. In other words, the electron spin polarization ratio based on the Boltzmann distribution is hopelessly tiny, and the measurement sensitivity in thermal equilibrium should be almost the same as that of ordinary electron spin resonance. However, as shown in Fig. 4b, most photo-excited electrons in the $|\pm1\rangle$ state relax to the ground state of $|0\rangle$ *via* intersystem crossing. The photoexcited electrons of $|\pm1\rangle$ also relax to the ground state of $|0\rangle$ *via* spin-allowed transitions, indicating that the photoexcitation cycle polarizes the triplet electron spin to the ground state of $|0\rangle$. The polarization rate exceeds 80% after photoexcitation cycles lasting from a few hundred nanoseconds to several microseconds.[83] This optical polarization process, often called "initialization," is generally used to reset the state to its initial state, $|0\rangle$. Consequently, magnetic resonance measurements of optically polarized NV centers can achieve sensitivity levels comparable to fluorescence detection. Indeed, the spin resonance of individual NV centers can be easily observed using a confocal fluorescence microscope stage.[17]

2.8. NV centers as a quantum sensor

To use NV centers as a quantum sensor, the perturbation to NV centers from the microenvironment is measured as spin population after certain spin manipulations and time evolutions.[88] For examples of spin manipulation, the temperature is determined by using the spin resonance frequency spectrum obtained by continuous-wave ODMR (CW-ODMR).[18,21,26,87] DC magnetic field is evaluated by measuring the spin magnetization precession by Ramsey fringe measurement (so-called "free induction decay (FID)").[36,89] Microenvironmental pH and radical are obtained from the longitudinal relaxation time T_1 measured by the inversion/saturation recovery method (T_1 relaxometry).[90–93] AC magnetic field is detected based on transverse relaxation time T_2 by Hahn echo or dynamic decoupling (T_2 relaxometry).[10,30]

The acquisition of spin magnetic frequency spectra (Fig. 4c–f) is currently the most frequently used method in life measurements. The measurement procedure is simple: continuous microwaves (or microwave pulses with a pulse width equivalent to a π pulse) are irradiated while sweeping the frequency. When the NV center is at a non-resonant microwave frequency (off-resonance), the spin population of $|0\rangle$ is more than 80%, whereas at a resonant microwave frequency (on-resonance), the spin population of $|0\rangle$ decreases due to spin excitation from $|0\rangle$ to $|\pm1\rangle$. The resonance frequency can be obtained by plotting the fluorescence intensity against the applied microwave frequencies (this plot is called "spin resonance frequency spectrum" or simply "ODMR spectrum") because a decrease in fluorescence intensity is observed at on-resonance. Since the resonance frequency is equivalent to the energy level derived from Hamiltonian (1), this measurement allows us to know the external electric and magnetic fields, as well as the temperature that affects the spin–spin interaction through the expansion and contraction of the crystal lattice, from the ODMR spectrum.[94]

2.9. Application of NV centers to magnetic field detection

In addition to obtaining ODMR spectra, another method for obtaining the resonance frequency of NV centers is the Ramsey fringe measurement (Fig. 5a–c), in which a microwave pulse orthogonal to the external magnetic field (z-axis) is applied to obtain information on the precession of spin magnetization in the xy-plane. The information obtained is similar to FID's in pulsed Fourier NMR (nuclear magnetic resonance) when an $\pi/2$ pulse is applied. However, unlike NMR, in the Ramsey fringe measurement of NV centers, the spin precession is detected based on the fluorescence intensity, not the induced electromotive force generated in the coil by electromagnetic induction. For this purpose, information on the spin precession should be converted into information on the number of spin occupations, which can be detected as the fluorescence intensity with high sensitivity. This is achieved by applying a second $\pi/2$ pulse to the electron spins after the free precession time τ and transferring the x-axis (or y-axis) component of the spin magnetization vector to the z-axis component (= spin quantization axis). This makes it possible to detect the phase of the spin magnetization at time τ based on the population of each spin magnetic quantum number, and by sweeping time τ as well, an NMR-like FID can be obtained. The Fourier transform of this FID yields the resonance frequency of the NV centers. However, while pulse Fourier NMR is overwhelmingly more useful than CW-NMR, in the case of NV centers, the use of ODMR spectra or FID depends on the purpose and experimental conditions. This is because, in the case of pulsed Fourier NMR, it is possible to obtain a spectrum of the required frequency band in a single shot of radio frequency pulse, which is a forward-compatible alternative to CW-NMR. In contrast, it is difficult to excite the required frequency band by a single shot of microwave pulse in the case of NV centers. Moreover, a sweep of time τ is also required because it is necessary to break the precession and convert the phase information into spin magnetic quantum number information. In addition, when using a nanodiamond as a probe, it is often necessary to acquire spectra in the absence of an external magnetic field (= zero magnetic field) for temperature measurements because the resonance frequency changes due to the free rotation of the nanodiamond. Therefore, Ramsey fringe measurements cannot alternate the acquisition of ODMR spectra by CW-ODMR. On the other hand, Ramsey fringe measurement has become an indispensable technique in high-sensitivity quantum sensor technology, for example, the D-Ramsey pulse sequence that cancels the effect of magnetic field fluctuations[95,96] and the use of two-quantum pulse sequences and spin-bath driving (decoupling from bus spins)[89,97] for high sensitivity magnetic field measurement. Its

 This journal is © The Royal Society of Chemistry 2025

Open Access Article. Published on 28 Januarie 2025. Downloaded on 2026-01-31 2:57:56 nm..
This article is licensed under a Creative Commons Attribution-NonCommercial 3.0 Unported Licence.

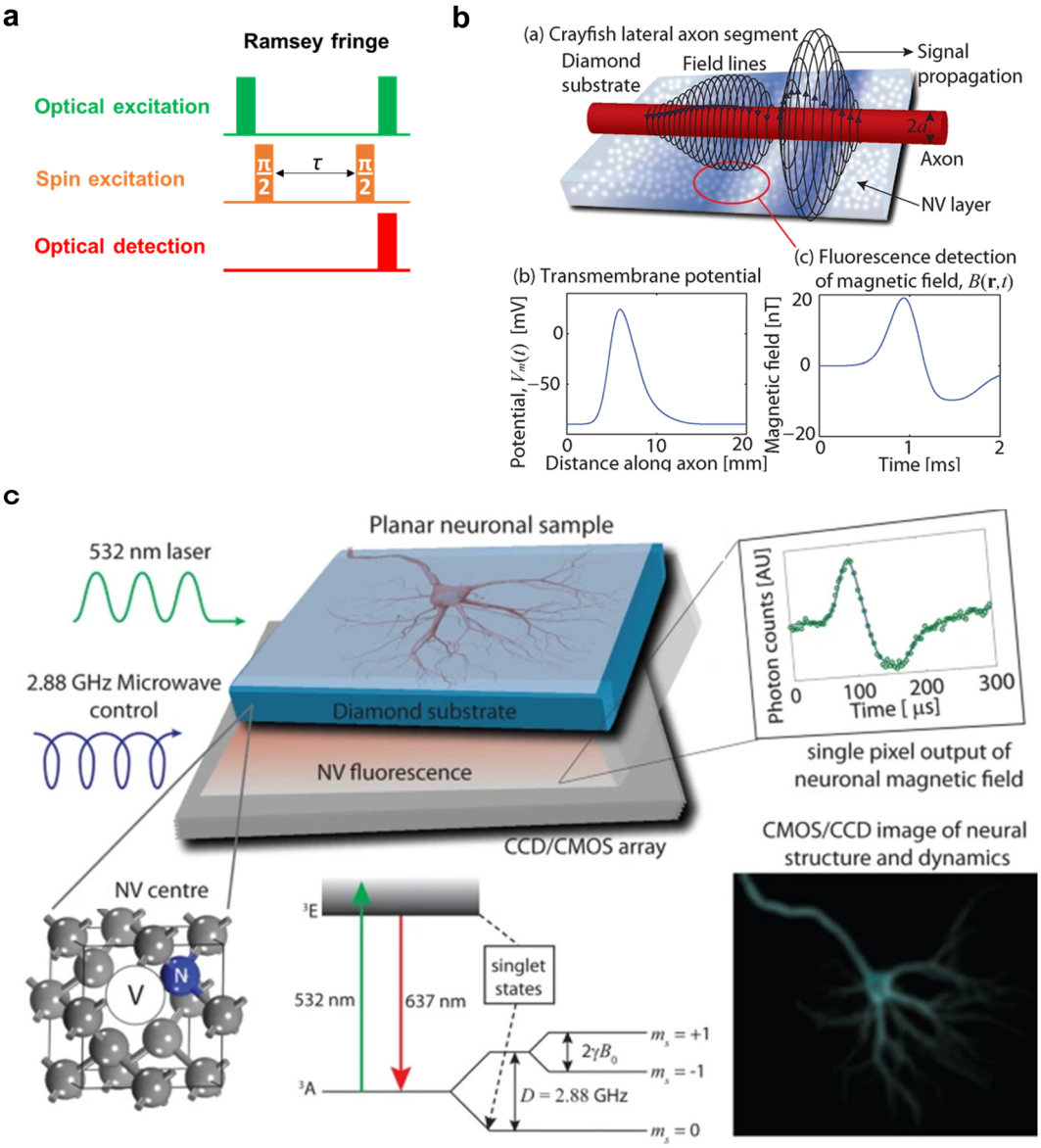

Fig. 5 Examination of biometric measurements using Ramsey fringe. (a) A typical pulse sequence of Ramsey fringe. (b) Schematic representation of the magnetic field generated by a neuron. The illustration depicts an axon positioned on a diamond substrate. The "Potential" refers to the vertical change in membrane potential (V_m) of a crayfish lateral axon, as cited from Watanabe *et al.* (*J. Gen. Physiol.* 1961, **45**, 267–308). The excitation propagates along the axon, resulting in time-dependent changes in the magnetic field at a distance of 100 nm. (c) Outline of neural measurements utilizing the NV center. The NV center's spin, controlled by a 2.88 GHz microwave, is perturbed by the magnetic field generated by the axon. These changes can be monitored based on the intensity of red fluorescence using a CCD or CMOS camera. Fig. 5b and c were reproduced from ref. 98 with permission from Springer Nature, copyright 2012.

application to life measurements is expected to accelerate in the future. However, Ramsey fringe measurements can be used to achieve higher sensitivity in temperature measurements, for example, by using D-Ramsey pulse sequences that cancel the effects of magnetic field fluctuations,[89,90] and higher sensitivity in magnetic field measurements by using two-quantum pulse sequences and decoupling from bus spins (spin-bath driving),[89,97] have become indispensable techniques in high-sensitivity quantum sensing, and their application to life measurements is expected to accelerate in the future.

2.10. Application of NV center to pH detection

Inversion/saturation recovery T_1 relaxometry (Fig. 6a–d) is a measurement method currently being applied to life science. The inversion/saturation recovery method is a measurement technique that monitors the relaxation from the thermal equilibrium state until the inverted or saturated spins return to the thermal equilibrium state again (spin–lattice relaxation, longitudinal relaxation). This measurement is often called T_1 relaxometry because the time constant for this relaxation has a name: longitudinal relaxation time T_1. T_1 is particularly

Open Access Article. Published on 28 Januarie 2025. Downloaded on 2026-01-31 2:57:56 nm..
This article is licensed under a Creative Commons Attribution-NonCommercial 3.0 Unported Licence.

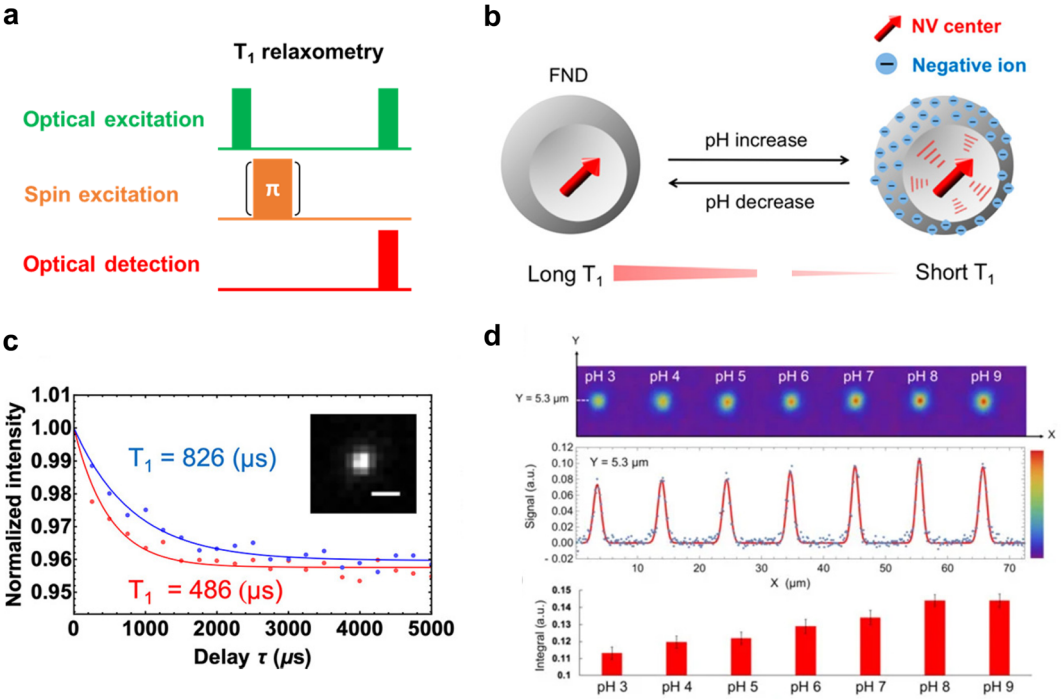

Fig. 6 Example of pH measurement using T_1 relaxometry. (a) A typical pulse sequence for T_1 relaxometry. (b) Mechanism of T_1 shortening with the rise in pH in surface-carboxylated fluorescent nanodiamonds. The carboxyl groups become negatively charged due to deprotonation as the pH increases.[91] (c) Decay of T_1 in the NV centers of carboxylated fluorescent nanodiamonds under different pH conditions.[91] The inset shows the fluorescent nanodiamonds with a scale bar of 1 μm. (d) T_1-Enhanced fluorescence images of carboxylated nanodiamonds (particle diameter 100 nm) under various pH conditions (top row) and corresponding signal intensity plots (middle row). The red line represents the results of curve fitting using a Gaussian function. The bottom row shows the integral of the fitted Gaussian function for each pH condition. Error bars represent the standard error from Gaussian fitting.[92] Fig. 6b–c and d were reproduced with permission from ref. 91 (ACS, copyright 2019) and ref. 92 (MDPI, copyright 2020), respectively.

sensitive to external magnetic and electrical influences and is known to be useful for measuring magnetic and radical concentrations (and related protein and cellular function).[19,99,100] It has also been recently reported that T_1 of NV centers in a nanodiamond can be used to measure microenvironmental chemical parameters such as pH with appropriate chemical modifications on the surface of the nanodiamond.[90,91] Because of its applicability to various measurements and simplicity of measurement, T_1 relaxometry is one of the most widely used measurement methods for life measurements using NV centers. In particular, simplicity of measurement is important for life measurements because biological samples such as cultured cells and animal tissues are generally delicate, and their conditions change from moment to moment. Therefore, it is necessary to start measurement as quickly as possible, omitting trial-and-error in advance as much as possible, and to obtain highly immediate information in a short measurement time. In addition, prolonged application of excitation light and microwaves can cause changes in the state of the samples, although the light and microwaves are low toxic to biological samples. Therefore, in pulsed ODMR measurements, such as Ramsey fringe measurements, for example, the determination of the $\pi/2$ pulse before the measurement is one of the obstacles to the development of the application to biological measurements. To determine the $\pi/2$ pulse, it is necessary to determine the resonance frequency in an appropriate magnetic field and perform a Rabi measurement. In contrast, T_1 relaxometry requires neither an external magnetic field nor microwave irradiation but only laser pulses to initialize the spins to $|0\rangle$ and read out the spin population to track the relaxation process. Furthermore, contrast imaging-like techniques provide high temporal resolution on the order of seconds,[92,101] making it an ideal measurement technique for biological measurements, with low toxicity to the biological sample and short measurement time.

2.11. Biological application of NV centers in nanodiamonds

Cellular temperature, pH, viscosity, and electric and magnetic fields are known as very important physicochemical parameters of the intracellular environment, as it has been pointed out that they may play a significant role in cell activity by affecting the dynamics and reactivity of biomolecules. Indeed, the increased activity of macrophages and immune cells during fever is one such example. In addition, cell division, gene expression, protein production, and metabolic activity have also been shown to be very closely related to cell temperature, pH, viscosity, and electric and magnetic fields,[102] and cell physicochemical parameters have become very important for understanding cell biological processes.

Therefore, NV centers in nanodiamonds that can measure physicochemical parameters (temperature, pH, viscosity, electric and magnetic fields, *etc.*), which largely reflect the cellular state, are useful. NV centers in nanodiamonds exhibit ODMR

 This journal is © The Royal Society of Chemistry 2025

Open Access Article. Published on 28 Januarie 2025. Downloaded on 2026-01-31 2:57:56 nm.. This article is licensed under a Creative Commons Attribution-NonCommercial 3.0 Unported Licence.

and can measure physicochemical parameters such as temperature from fluorescence intensity, pH from spin lifetime,[103] viscosity from fluorescence bright spot mobility, and magnetic field from the optical detection of Zeeman splitting. It has already been reported that it is possible to measure physicochemical parameters using the optical detection of Zeeman splitting. This method can be accelerated with widefield imaging[104] or integrated with chip-based microwave architecture for bioassay platforms.[105] Specifically, by measuring the temperature of stem cells using NV centers in nanodiamonds, it has been shown that the ability of stem cells to produce regenerative factors such as HGF and VEGF and their differentiation function changes significantly with temperature.[106] In addition, 3D tracking of the motor rotation of a motor protein (F1-ATPase), which is related to the efficacy of drugs, has been achieved by utilizing the magnetic field measurement capability of the NV center in nanodiamonds. Furthermore, nanodiamonds, including NV centers with carboxy groups on the surface, can measure pH in a tiny area inside a cell using the spin relaxation induced by pH change. By taking advantage of these quantum characteristics, the effects of physicochemical parameters of cells on the expression of their functions have not yet been fully elucidated, and the application to advanced biomedicine, such as cancer medicine, immunology, neuroscience, and regenerative medicine, is strongly anticipated. Recently, optoelectronical nanoparticles and 2D semiconductor nanomaterials are proactively utilized for the development of wearable health monitoring systems due to their unique properties, such as high sensitivity, flexibility, and biocompatibility.[107–109] Considering this trend, diamond NV centers have potential as they can be incorporated into wearable devices to provide real-time, non-invasive monitoring of key physiological parameters. Their stable fluorescence, ability to measure physical and chemical parameters, and integration with flexible sensing systems suggest that diamond NV centers could be adapted for health tracking in applications like continuous temperature monitoring, biochemical sensing, and real-time physiological assessments.

3. Quantum technology-based hyperpolarized MRI/NMR

3.1. Nuclear magnetic resonance spectroscopy and imaging

Since the first report on the nuclear magnetic resonance (NMR) phenomenon in the 1940s,[110,111] NMR spectroscopy has been established and used in various scientific fields such as chemical structure elucidation and drug/protein interaction analysis.[112] Magnetic resonance imaging (MRI), initially developed in 1973,[113] supports medical diagnostics, and its practical applications have been realized in (bio)chemical experiments and disease diagnosis by the manipulation of nuclear spins in the magnetic field using radio frequency (RF) pulses to obtain spectra or images. As a versatile quantum phenomenon-based technology, NMR/MRI has contributed to the progress of modern life sciences and medicine.

MR essentially employs an RF pulse, which exhibits high penetration in living organisms, to mainly excite the spins of water or lipid protons (^{1}H, nuclear spin $I = 1/2$) oriented in two possible directions within the magnetic field by Zeeman splitting.[114] The resulting relaxation process is detected from the resonator coil as a weak current (free induction decay (FID)) and then amplified and converted to NMR spectra or 2D/3D images using the Fourier transform. It should be noted that ''low sensitivity'' in the NMR phenomenon is a fundamental technical drawback, which can be attributed to the small difference in the population of the two energy states of nuclear spins following the Boltzmann distribution under thermal equilibrium, involved in MR signal detection (Fig. 7a and b).[114]

3.2. Nuclear hyperpolarization

Various techniques have been developed to improve the intrinsically low-sensitivity signals in MR to maximize its applications in the biochemical and biomedical domains, which can be categorized into ''nuclear hyperpolarization (HP)'' by dynamic nuclear polarization (DNP).[115] DNP is a powerful method for enhancing the sensitivity of NMR/MRI, and it has garnered significant attention in recent years. The original concept of spin diffusion can be backtracked to the theoretical background proposed by Albert Overhauser in 1953.[116] This interaction occurs between unpaired electrons and NMR-positive nuclei upon irradiation at the electron paramagnetic resonance (EPR) frequency, following the transfer of the excitation of electron spin energy to the nuclei and significantly enhancing the NMR signals of the nuclei. Subsequently, this phenomenon was experimentally demonstrated[117] and applied to 1D and 2D NMR techniques for inter- and intramolecular analyses. DNP in solid samples, mixed with unpaired radicals and NMR-positive nuclei, was accomplished in the 1980s and applied for molecular structural elucidation (nuclear Overhauser effect (NOE))[118] or solid-state NMR.[119] The DNP process can be described by three commonly accepted mechanisms, depending on experimental conditions, *i.e.*, the solid effect (SE), cross effect (CE), and thermal mixing (TM).[120] Applications of DNP have been extended to medical diagnostic imaging. Spin exchange optical pumping (SEOP) is a pioneering method in clinical HP measurement used to excite the nuclear spin of noble gas atoms (^{3}He, ^{129}Xe, *etc.*) by the direct collision of alkali metal atoms (Rb, *etc.*) whose unpaired electrons are excited by laser irradiation, thereby enhancing nuclear spin polarization by several tens of percent.[121,122] This gas-based HP method has been successfully approved as medical diagnostics for chronic obstructive pulmonary disease (COPD) or other lung-related diseases where the ^{1}H density is relatively low *in vivo*. Overhauser-enhanced MRI (OMRI), also known as proton electron double resonance imaging (PEDRI),[123] is a DNP-based method for enhancing intrinsically low-sensitivity NMR signals. A paramagnetic contrast agent with a narrow EPR linewidth is used as a host radical during exogenous injection and irradiated to excite its spin polarization; then, the polarization is transferred to ambient nuclear spins to enhance the NMR sensitivity. This imaging provides highly resolved anatomical information with EPR spectroscopic functional information such as partial pressure of oxygen (pO_2),[124] redox status,[125] microvascular permeability,[126] *etc.*

Open Access Article. Published on 28 Januarie 2025. Downloaded on 2026-01-31 2:57:56 nm..
This article is licensed under a Creative Commons Attribution-NonCommercial 3.0 Unported Licence.

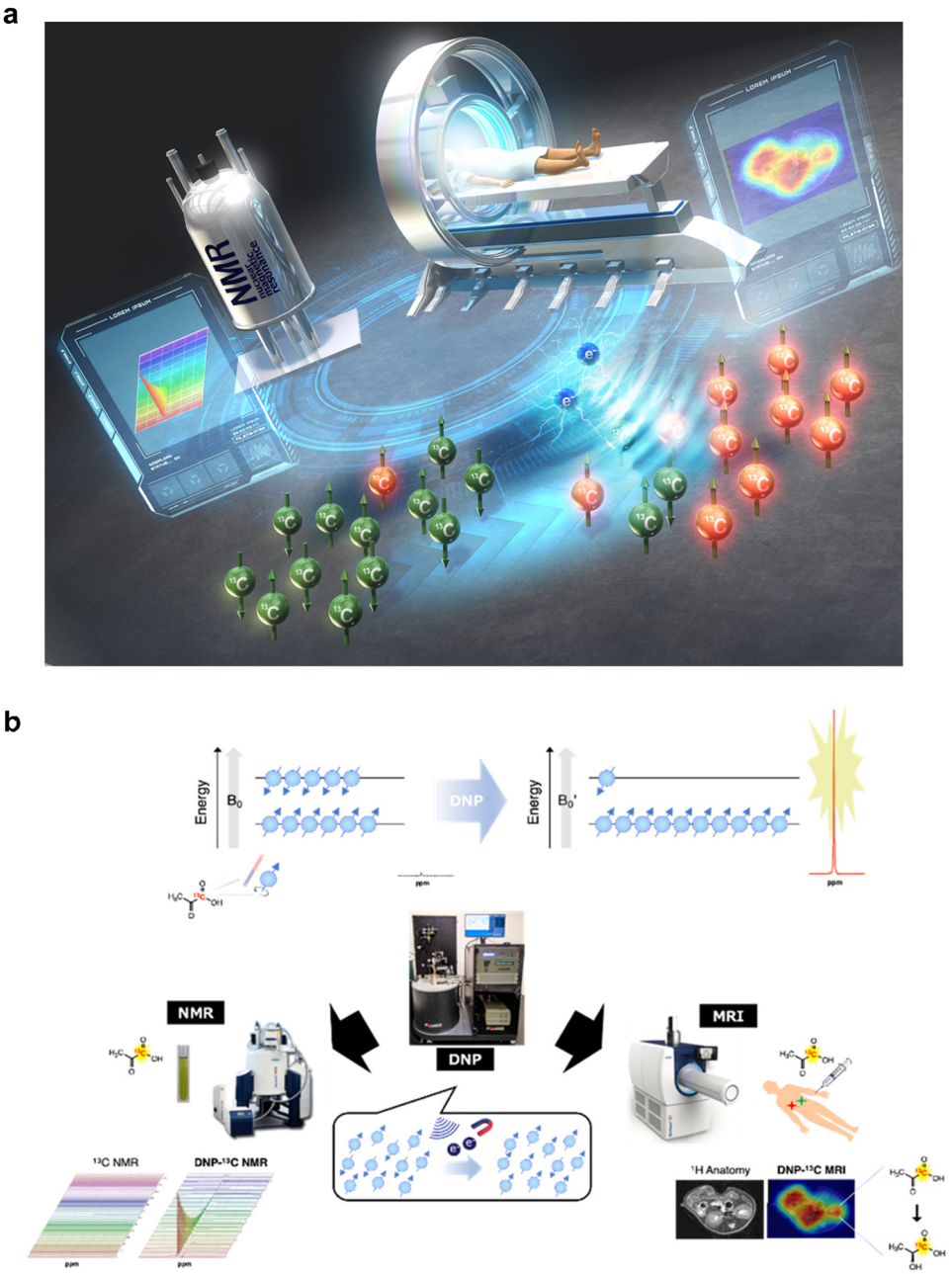

Fig. 7 Conceptual diagram of quantum technology-based hyperpolarized MRI/NMR and schematic of nuclear HP and subsequent measurement by NMR/MRI. (a) For the establishment of hyperpolarized NMR/MRI, benchtop-sized nuclear hyperpolarization (HP) machines without cryogen and much more sophisticated HP sites for clinical dissolution DNP (dDNP) technologies. (b) Nuclear spins (I = 1/2) align two possible directions within the magnetic field (B_0) by Zeeman splitting. The slight difference in the two energy states following the Boltzmann distribution under thermal equilibrium contributes to the resulting intrinsically "low-sensitivity" MR signals. The proliferation of nuclear spins by DNP increases the population difference in the two energy states, and the dissolution of the following sample generates aqueous samples without polarization loss. Quick sample delivery to detectors allows *in vitro* spectroscopy (left) or *in vivo* spectroscopic imaging (right) based on >10 000-fold enhanced MR signals (hypersensitive NMR/MRI). Fig. 7b was reproduced from Fig. 2 and 3 in Takakusagi Y. *Brain Neural Networks*, **30**(4), 179–188, with permission from the Japanese Neural Network Society, copyright 2023.

Parahydrogen-induced polarization (PHIP), which is not categorized as an Overhauser-type DNP, is an alternative way to induce nuclear spin polarization by the chemical adduction of parahydrogen.[127]

Parahydrogen is a nuclear spin isomer of hydrogen with magnetization. Owing to the hydrogenation reaction with unsaturated bonds in molecular probes with a catalyst and *via* field cycling in zero magnetic field chambers, the magnetization is transferred to labeled nuclear spins (^{13}C, ^{15}N, *etc.*) in the molecular probe to enhance the following MR signals.[128] The recent developments by SABRE or SABRE-SHEATH have accomplished PHIP in a reversible catalytic cycle at lower concentration levels in microtesla fields within a magnetic shield, thereby reducing the HP substrate required for NMR/MRI

 This journal is © The Royal Society of Chemistry 2025

Open Access Article. Published on 28 Januarie 2025. Downloaded on 2026-01-31 2:57:56 nm.
This article is licensed under a Creative Commons Attribution-NonCommercial 3.0 Unported Licence.

measurements.[129–132] A commercial PHIP polarizer has recently been developed for preclinical and clinical studies (POLARIS, NVision Imaging Technologies GmbH, Germany). In addition, various molecular probes containing intramolecular unsaturated chemical bonds or introducing unsaturated bonds using a "side arm" for hydrogenation (SAH) in molecules have contributed to the expansion of PHIP utilization.[133]

3.3. Dissolution-DNP (dDNP)

In 2003, Ardenkjær-Larsen *et al.* developed an innovative apparatus for obtaining HP aqueous samples. This technique allows the rapid dissolution of highly polarized solid samples as a liquid with suitable temperature and minimal polarization loss, enabling the injection of living bodies to detect spectroscopic signals or metabolic reactions based on >10 000-fold enhanced signals compared to the thermal equilibrium value.[134] For a nucleus with spin = 1/2, the polarization level can be expressed by the Maxwell–Boltzmann statistics:

$$P \equiv \frac{N^- N^-}{N^+ N^-} = \tanh\left(\frac{\gamma \hbar B_0}{2kT}\right) \quad (2)$$

Here, N^+ and N^- denote the number of spins in the up and down directions, respectively; moreover, B_0 is the magnetic field strength, γ is the gyromagnetic ratio of the nucleus, T is the temperature, k is the Boltzmann constant, and $\hbar$ is the Dirac constant.[114] To increase the population difference in two energy states, *i.e.*, to create an HP state, a stronger magnetic field and cryogenic temperature are required.

Experimentally, low-molecular-mass compounds (MW ~200) labeled with NMR-positive nuclei, such as ^{13}C or ^{15}N, are dissolved in a glassing agent doped with an electron paramagnetic agent (EPA). The mixture is conditioned in a cryogenic magnetic environment (3.35–7 T, 0.7–1.5 K); subsequently, owing to the irradiation of unpaired electrons with microwaves, the spin polarization is transferred from the electrons to the nuclei, which can be monitored as polarization buildup *via* solid-state NMR. These polarized samples must be dissolved in a superheated buffer to warm up to around the biological temperature, maintaining the polarization, physiological pH, and isotonicity. The resulting solution is subjected to NMR/MRI for *in vitro* spectroscopy or *in vivo* imaging using enhanced MR signals (Fig. 7a and b).

Unlike other MRI techniques, longitudinal relaxation by HP magnetization is nonrecoverable after dissolution from the magnetic field in the hyperpolarizer. The longitudinal magnetization, $M_z(t)$, can be represented as:

$$\begin{aligned} M_z(t) &= M_0 + \left(M_{z,\mathrm{HP}} - M_0\right)\exp\left(-\frac{t}{T_1}\right) \\ &\equiv M_{z,\mathrm{HP}}\exp\left(-\frac{t}{T_1}\right) \end{aligned} \quad (3)$$

where $M_{z,\mathrm{HP}}$ is the initial HP magnetization, M_0 is the thermal equilibrium magnetization, and T_1 is the longitudinal relaxation time. Generally, the value of T_1 of HP signals from ^{13}C-labeled compounds developed as probes is approximately 30–60 s, depending on the local chemical environment of the molecular structure; it requires the quick delivery of HP samples to the detector in a dedicated facility for HP measurement.

Thus far, several polarizers have been commercially developed to realize dDNP in typical laboratory environments. The apparatus of the prototype polarizer (3.35 T) contained a manual dissolution system with a dissolution wand.[134] In 2006, HyperSense™, an automated hyperpolarizer (HyperSense™, Oxford Instruments, 3.35 T, 94 GHz, 1.4 K), was developed, and by 2009, over 40 machines had been sold. In 2011, a polarizer for viewing real-time cell activity (SPINlab™, GE Research Circle Technology, 5 T, 140 GHz, 0.7 K) was introduced; this machine exhibited high throughput and was fully automated with fluid-path sample dissolution equipped with four channels (*i.e.*, up to four samples can be simultaneously polarized in parallel).[135] SPINlab™ was later transformed into a clinical hyperpolarizer with a quality control (QC) unit, and there are currently over 25 machines worldwide.[136] More than 100 clinical studies have been conducted on the dissolution of DNP for future metabolic imaging.[137,138] In 2018, a state-of-the-art cryogen-free hyperpolarizer (SpinAligner™, 6.7 T, 1.3 K) was commercially launched by Polarize IVS (Denmark).[139] As of 2023, 15 SpinAligner machines have been installed globally. Furthermore, homemade polarizers[140–143] or brute force polarization that enforces nuclear spin polarization in the sub-milli K temperature range has been developed and used for HP studies.[144]

3.4. Application for metabolic imaging

The advent of the dDNP technique has resulted in forming a new academic discipline, *i.e.*, real-time metabolic imaging. Its application was first reported in rats and pigs. Golman *et al.* reported real-time monitoring of the metabolic fate of $^{13}C_1$-enriched hyperpolarized pyruvate by detecting lactate, alanine, and bicarbonate as metabolites.[145,146] Pyruvate is produced at the intersection of oxidative phosphorylation (OXPHOS) and anaerobic fermentation. In normal tissues, pyruvate enters mitochondrial metabolism, generating 36 ATPs in total *via* OXPHOS. In cancerous or inflamed tissues, pyruvate metabolism shifts from OXPHOS to lactate generation in the cytosol by increasing aerobic glycolysis due to elevated lactate dehydrogenase (LDH) activity, known as the Warburg effect.[147] This metabolic shift is highly correlated with malignant transformation and therapeutic response in cancer, and a significant increase in the conversion of HP [1-^{13}C]pyruvate to lactate can be a potential metabolic biomarker.[148] *In vivo* imaging studies have been conducted for healthy and diseased rodent models as preclinical research.[149] Furthermore, this metabolic imaging has been successfully integrated into preclinical and clinical cancer research for the diagnosis of aggressiveness or prognosis of prostate cancer, renal cell carcinoma, hepatocellular carcinoma, glioma, pancreatic cancer, breast cancer, therapeutic response upon treatment with inhibitors, anti-angiogenesis, hypoxia-activated prodrugs, X-irradiation, androgen cessation therapy, and cancer immunotherapy.[135,137,138,150] Its neurological applications in healthy human brains, age, sex, effects of anesthesia, cellular studies of immunometabolism, and primary brain diseases have also been investigated.[151] Moreover, the metabolism in other lifestyle diseases, such as heart, kidney, diabetes, liver, and

Open Access Article. Published on 28 Januarie 2025. Downloaded on 2026-01-31 2:57:56 nm.
This article is licensed under a Creative Commons Attribution-NonCommercial 3.0 Unported Licence.

non-alcoholic fatty liver disease and liver fibrosis, has been examined to validate the disease state.[151]

3.5. Molecular probes

Since the demonstration of [1-^{13}C]pyruvate as a promising molecular probe for detecting metabolic reprogramming as a hallmark of cancer, studies on potential metabolic biomarkers have generated various functional molecular probes.[152–154] These include [1,4-$^{13}C_2$]fumarate for detecting tumor necrosis, [1-^{13}C]dehydroascorbic acid for redox monitoring, [1-^{13}C]alpha-ketoglutarate for IDH1 activity in glioma, [1-^{13}C]glycerate for assessing glycolysis, ^{13}C-urea and $^{15}N^{+}$-α-trideuteromethylglutamate for HP perfusion imaging, and [^{13}C]bicarbonate as a pH sensor.[152–154] Furthermore, the *de novo* design of molecular probes has generated [1-^{13}C]pyruvate ethyl ester for metabolic imaging in rat brains, ^{13}C-benzoyl formic acid and ^{13}C-thiourea for H_2O_2 detection, ion chelators as *in vitro* metal sensors, and *in vitro* and *in vivo* pH sensors.[152–154] Amino acids are components of the body and are attractive templates of the HP molecular probe with higher solubility and less toxicity.[155] The amino acid-based molecular probes that maintain a longer HP lifetime in carbonyl carbon (position 1) and modified side chains were generated. These include [5-^{13}C]glutamine for probing the glutaminase activity and treatment response, [5-^{13}C]glutamate for imaging biomarker for IDH1 mutational status in glioma, aspartate, glycine, serine and their derivatives labeled with ^{13}C at the C-1 position and [1-^{13}C]lysine ethyl ester for pH sensor, [6-^{13}C,$^{15}N_3$]arginine for *in vivo* arginase activity.[152–154] Furthermore, [1-^{13}C]alanine was applied for non-invasive assessment of telomere maintenance mechanisms in brain tumors,[156] [1-^{13}C]alanine amide for detecting aminopeptidase N (APN) activity[157] and simultaneous evaluation of renal physiological state,[158] and [1-^{13}C]*N*-acetyl cysteine to monitor glutathione redox chemistry.[159] The recent development of peptide-based molecular probes (γ-Glu-[1-^{13}C]Gly) has enabled the direct monitoring of γ-glutamyl transpeptidase (GGT) activity.[160,161] In particular, Ala-[1-^{13}C]Gly-d_2-NMe_2, the second generation of APN probes that enabled *in vivo* APN activity, possess "self-glassing" characteristics, similar to pyruvate;[162] in other words, glassing agents (glycerol, DMSO, or others) necessary for DNP, which are possibly toxic to living organisms in some cases, are not required. Recently, an optimal glutamine probe, [5-^{13}C,4,4-d_2,5-^{15}N]-L-glutamine, which prolonged ^{13}C relaxation at position 5, successfully monitored the *in vivo* glutamine metabolism in pancreatic cancer.[163]

To generate functional HP molecular probes, it is important to design molecules with longer HP lifetimes and target specificity, including enzymes or various physiological states. The T_1 value is generally correlated with the HP lifetime and is often used as its index. The relationship between the nuclear spin state and the molecular structure surrounding the nuclei can be understood according to the relaxation theory, as indicated by the following equation:

$$\frac{1}{T_1} = \frac{1}{T_{1\mathrm{DD}}} + \frac{1}{T_{1\mathrm{CSA}}} + \frac{1}{T_{1\mathrm{SR}}} + \frac{1}{T_{1\mathrm{SC}}} + \frac{1}{T_{1\mathrm{other}}} \quad (4)$$

Here, DD represents the dipole–dipole interaction between HP ^{13}C and ^{1}H, CSA is the chemical anisotropy that depends on the orientation of the molecule in the static magnetic field, SR is the spin rotation of a covalent bond connected to labeled and other atoms, and SC is the Scholar coupling with neighboring atoms. It should be noted that the precise investigation of the extent of each relaxation factor is a guideline for minimizing the relaxation factors and rationally designing functional molecular probes that can maintain longer HP lifetimes for labeled nuclear spins for *in vivo* imaging.[152] Following this theory, ^{13}C-labeled *t*-Bu benzene[164] and ^{15}N-labeled trimethylphenyl ammonium (TMPA)[165,166] were rationally designed, indicating the longest HP lifetime (sulfonated ^{13}C *t*-Bu benzene in D_2O: 209 ± 7 s (9.4 T, 37 °C), [^{15}N, D_{14}]TMPA in D_2O: 1177 ± 52 s (9.4 T, 30 °C)) among the HP probes of small molecules.

3.6. Other applications

In addition to developing instrumentation, various techniques and applications have been designed to maximize HP efficiency and reduce the complexity of HP measurements. These include automatic sample transfer from the polarizer to detector,[167] construction of magnetic shield tunnels to maintain HP signals in molecular probes during transfer,[168] and transferring hyperpolarized solid samples.[169] Furthermore, the addition of trace amount of Gd ions to DNP sample formulation has been studied for enhancing the polarization,[170,171] deuteration of EPA and glassy matrix to discard dipole–dipole interactions,[172] DNP without glassing agent,[173] UV irradiation for ^{13}C probes to generate non-persistent radicals used for DNP,[174,175] porous functional materials (HYPOP or HYPSO) to immobilize EPA for DNP and eliminate the process of EPA removal before injection into the living body,[176,177] and transport metabolites from large-scale HP centers to end users in remote dedicated sites.[178,179] Challenges to *in vitro* use were also analyzed, which could not otherwise be experimentally investigated, including the direct monitoring of cell metabolism, use of cell bioreactors, or tissue slice bioreactors, spheroids, brain organoids, and organs.[151,180–182] Moreover, drug–protein interactions have been validated *via* DNP-NMR.[183,184]

3.7. HP at room temperature

As mentioned earlier, the development of SEOP or PHIP enabled the nuclear HP of noble gases or functional molecular probes at room temperature without expensive cryogens.[185] The development of dDNP with cryogen-free techniques has helped expand the use of HP metabolic imaging in preclinical and clinical sites with access to existing MRI scanners. Although the electron spin polarization is only 0.76% at 298 K in 3.35 T, photoexcited electron triplet states, which do not follow the Boltzmann distribution, resulted in HP at room temperature.[186,187] Using lasers with an appropriate wavelength, pentacene in the excited singlet state could be converted to the triplet state through intersystem crossing, thereby exhibiting more polarization than the thermal equilibrium state.[188] The polarization was then transferred to short T_1 nuclei (*e.g.*, ^{1}H) following the labeled nuclei (*e.g.*, ^{13}C) in benzoic acid, regardless of the range of temperature or strength of magnetic field.[189] While signal amplification using this technique was

 This journal is © The Royal Society of Chemistry 2025

Open Access Article. Published on 28 Januarie 2025. Downloaded on 2026-01-31 2:57:56 nm.
This article is licensed under a Creative Commons Attribution-NonCommercial 3.0 Unported Licence.

generally achieved with single or co-crystals of host–guest molecules, the recent developments allowed sample dissolution without polarization loss, thus broadening the scope of this technique.[190,191] Nevertheless, triplet-DNP measurements are limited by the magnitude of signal amplification, mainly due to the low solubility of pentacene or the limited characteristics of guest molecules available for this polarization. To expand the utility of these techniques, several challenges have been reported *via* material development, such as the use of a metal–organic framework (MOF) composite containing pentacene, the generation of more dispersible pentacene derivatives, and the use of porphyrin as a biocompatible polarizing agent.[192,193] Meanwhile, host medicinal agents or biological components can be used as the guest molecule for measuring triplet-DNP.[194–196] Recently, the spin polarization of quintet multiexcitons generated by singlet fission (SF) has been reported to improve the sensitivity of MR of water molecules through DNP, indicating the utility of SF as a polarized spin generator in the bio-quantum technology.[197] Moreover, drug–protein interaction analysis has also been achieved *via* triplet DNP-NMR.[198] Further studies can improve the performance of the HP technique at room temperature.

3.8. Perspectives

Among the various available medical diagnostic imaging techniques, MRI is the only method that employs a quantum phenomenon as the detection principle based on nuclear spin manipulation and detects the relaxation process. This signal allows the monitoring of molecular structural changes in metabolites using the nuclear frequency of the NMR-positive nuclei as the chemical shift alteration at arbitrary magnetic field strength. Combined use with nuclear HP is only possible in this quantum-based imaging technique to improve the sensitivity. Moreover, utilizing the difference in the observed spin frequency, single or multiple molecules can be simultaneously detected within several tens of seconds of a single scan.[199–201] Further, combined use with other modalities (*e.g.*, HyperPET combined with FDG-PET)[199,202] will improve the clinical diagnostic accuracy by monitoring the tissue metabolism in the disease state or therapeutic response (metabolotheranostics).[203] Even in the field of life sciences, dDNP will contribute to basic studies in various fields such as cancer, neurological studies, lifestyle diseases, regenerative medicine, and drug discovery studies targeting intrinsically disordered proteins in cellular milieus.[204,205] The development of HP molecular probes in each type of nuclear HP modality will also expand the utility of the approach.[206] Technical developments, *e.g.*, benchtop-sized HP machines without cryogen or much more sophisticated HP sites, will facilitate the application of preclinical and clinical dDNP technologies to establish hypersensitive NMR/MRI.

4. Quantum biology and quantum biotechnology

4.1. Quantum biology

Quantum biology is a new interdisciplinary scientific field that applies quantum principles such as the tunnelling effect, quantum superposition, quantum entanglement, and coherence to study processes in biological systems that are difficult or impossible to describe using classical physical laws alone. At present, magnetoreception, energy transfer in photosynthesis, olfaction, and enzymatic reactions are the main research subjects of quantum biology (Fig. 8). However, it is challenging to detect such effects because quantum effects may have little to no impact on biological processes in warm and wet living systems because the biological environment quickly causes dissipation and decoherence of the quantum system. Previously, olfaction was considered to depend on the shape and size of odorants fitting an olfactory receptor. However, the odorant of which hydrogen was substituted with deuterium resulted in odor change, suggesting vibrational frequency might play a role in the olfaction.[207] Experiments with inelastic electron tunneling spectroscopy were carried out to validate and examine the proposed vibrational theory of olfaction. However, it is still controversial.[208,209] In this chapter, we focus on the magnetoreception of migratory birds and photosynthesis in plants, which are currently well-studied as representative examples of research topics in quantum biology.

4.2. Radical pair mechanism in magnetoreception

Magnetoreception is the ability of organisms to receive geomagnetic information used for orientation, migratory, homing, feeding, breeding, *etc.* Many species, including birds, mammals, reptiles, amphibians, fish, crustaceans, insects, and plants, have been reported to have the magnetoreception.[210] Since the 2000s, cryptochromes (CRYs), which are highly conserved blue light–absorbing flavoproteins containing a flavin adenine dinucleotide (FAD), have been attracting researcher's attention as possible quantum sensors of magnetoreception.[211,212] CRYs in many species, such as CRY4s of *Erithacus rubecula* (European robin),[213] *Columba livia* (pigeon),[214] *Gallus gallus* (chicken),[215–217] CRY1a of *Sylvia borin* (garden warbler),[218] CRY of *Drosophila melanogaster* (fruit fly),[219,220] CRY1 and CRY2 of *Danaus plexippus* (monarch butterfly),[219] CRY2 of *Periplaneta americana* (cockroach),[221] CRY1 of *Arabidopsis thaliana*,[222–224] *etc.* have been proposed to act as magnetosensors.

The fundamental principle of the CRY magnetosensor is that the long-lived spin-correlated radical pair (RP) generated in CRY detects the angle of the magnetic field.[212–214,216,217,220,223,225–227] The reaction schemes of avian CRY4s proposed from previous studies are summarized in Fig. 9a. When the blue light or UV irradiates the oxidized FAD (FADox) of the grand state in CRY, an excited singlet state of FAD (^{S}[FAD*]) is produced. Then, the electron transfer from three or four tryptophans (TrpA395, TrpB372, TrpC318, and TrpD369 conserved in CRY4s of *E. rubecula*, *C. livia*, and *G. gallus*) to FAD is induced sequentially, and radical pairs (RP_A, RP_B, RP_C and RP_D) consisting of FAD and Trps are formed. In this reaction scheme, high-rate constants of $RP_A \rightarrow RP_B$ and $RP_B \rightarrow RP_C$ lead RP_C and RP_D that form the composite RP due to the dynamic equilibrium of $RP_C \leftrightarrow RP_D$. This composite RP is in a spin-correlated state consisting of an anion FAD radical ($FAD^{\bullet -}$) and a cationic Trp radical ($TrpH^{\bullet +}$),[213] which can oscillate between electronic singlet (S)

Open Access Article. Published on 28 Januarie 2025. Downloaded on 2026-01-31 2:57:56 nm..
This article is licensed under a Creative Commons Attribution-NonCommercial 3.0 Unported Licence.

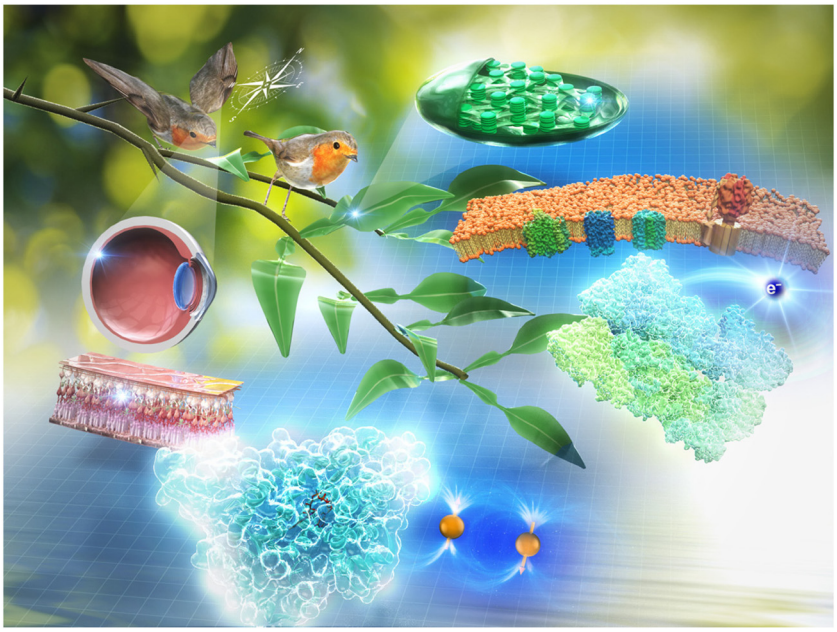

Fig. 8 Conceptual diagram of quantum biology and quantum biotechnology. Quantum effects which play a critical role in a variety of biological functions, including photosynthesis, magnetoreception, and enzymatic reactions. Their mechanisms are not well understood and are a hot topic in quantum biology.

state (^{S}[FAD$^{\bullet-}$ TrpH$^{\bullet+}$]) and triplet (T) state (^{T}[FAD$^{\bullet-}$ TrpH$^{\bullet+}$]) under the influence of intramolecular electron–nuclear hyperfine interactions (''Intersystem crossing A'' in Fig. 9a). The relative angle between the external magnetic field line and the composite RP can affect the extent and frequency of the S–T mixing process, which could alter the quantum yield of the subsequent, stabilized RP (^{S,T}[FADH$^{\bullet}$ Trp$^{\bullet}$] in Fig. 9a) that consists of a neutral semiquinone radical (FADH$^{\bullet}$) and a neutral Trp radical (Trp$^{\bullet}$).[218,228,229] Several spectroscopic analyses, such as transient absorption analysis near 50 μT, revealed that the reaction process from the composite RP to the stabilized RP proceeds over a time scale of 1 to 10 μs.[213,225] This time scale is longer than required to receive geomagnetic information (approximately one μs *in vivo*).[225] The quantum yield of the stabilized RP altered by the magnetic field effect could trigger the magnetic signaling from CRY4 to the nervous system, probably through the assistance from Tyr319, the conformational change in the C-terminal tail accompanying the change in the interaction to unknown CRY receptors.[216,217,230] This RP mechanism also called the ''CRY hypothesis,'' is now widely believed to be the first step in geomagnetic sensing.[213,216,231–233]

4.3. Universality of CRY hypothesis in magnetoreception

Even focusing on the avian CRY4s again, processes other than those described in Section 4.1 have been reported. For example, the highly conserved Tyr319 (colored in grey in Fig. 9a) may lead to the formation of RPs consisting of [FAD$^{\bullet-}$ Tyr-O$^{\bullet}$] with highly long lifetimes (tens of microseconds or more).[216,227] However, it remains unclear whether these RPs constitute entangled states and how they contribute to magnetoreception. The existence of RP formed by FADH$^{\bullet}$ and superoxide $O_2^{\bullet-}$, which can oscillate between S–T states (''Intersystem crossing B'' in Fig. 9a), was also reported.[227,234,241] This process may relate to the signaling in the dark condition;[227] however, there may be another additional process before the signaling because the extremely fast spin relaxation in $O_2^{\bullet-}$ is unsuitable as a magnetosensor.[234] Moreover, not only CRY4 but also CRY1a in birds have a magnetic sensitivity,[242,243] whereas the identity of RP of CRY1a has not yet been elucidated.[224,244–249] Also, vertebrate CRY1a, including birds, seems not to bind FAD strongly *in vitro*.[248,250]

In invertebrates, the situation is more complicated. The magnetic-dependent binary-choice behavioral assay using *D. melanogaster* revealed that the CRY-defective mutant flies lost their magnetoreception, indicating that CRY is required for the magnetoreception of *D. melanogaster*.[251] Surprisingly, a recent study showed that the 52 C-terminal amino acid residues (CT) of *D. melanogaster* CRY, lacking the canonical FAD-binding domain and Trp residues, were sufficient to facilitate magnetoreception *in vivo*.[252] Moreover, several studies suggested that molecules other than CRY, probably high levels of FAD alone, could generate magnetically sensitive RPs and produce a biological effect under appropriate conditions.[252–254] These observations suggested that *D. melanogaster* CRY-CT acts as an adaptor, bringing photoactivated FAD close to other effector molecules, including unknown CRY receptors.[235–238,252]

Despite many continuous discoveries, it still needs to entirely explain the magnetoreception based only on current knowledge. The perceptual mechanism of magnetic information is likely to be diverse across species and may be difficult to understand in line with human sensory modalities. Although we have gradually accumulated physical and biological knowledge

 This journal is © The Royal Society of Chemistry 2025

Open Access Article. Published on 28 Januarie 2025. Downloaded on 2026-01-31 2:57:56 nm..
This article is licensed under a Creative Commons Attribution-NonCommercial 3.0 Unported Licence.

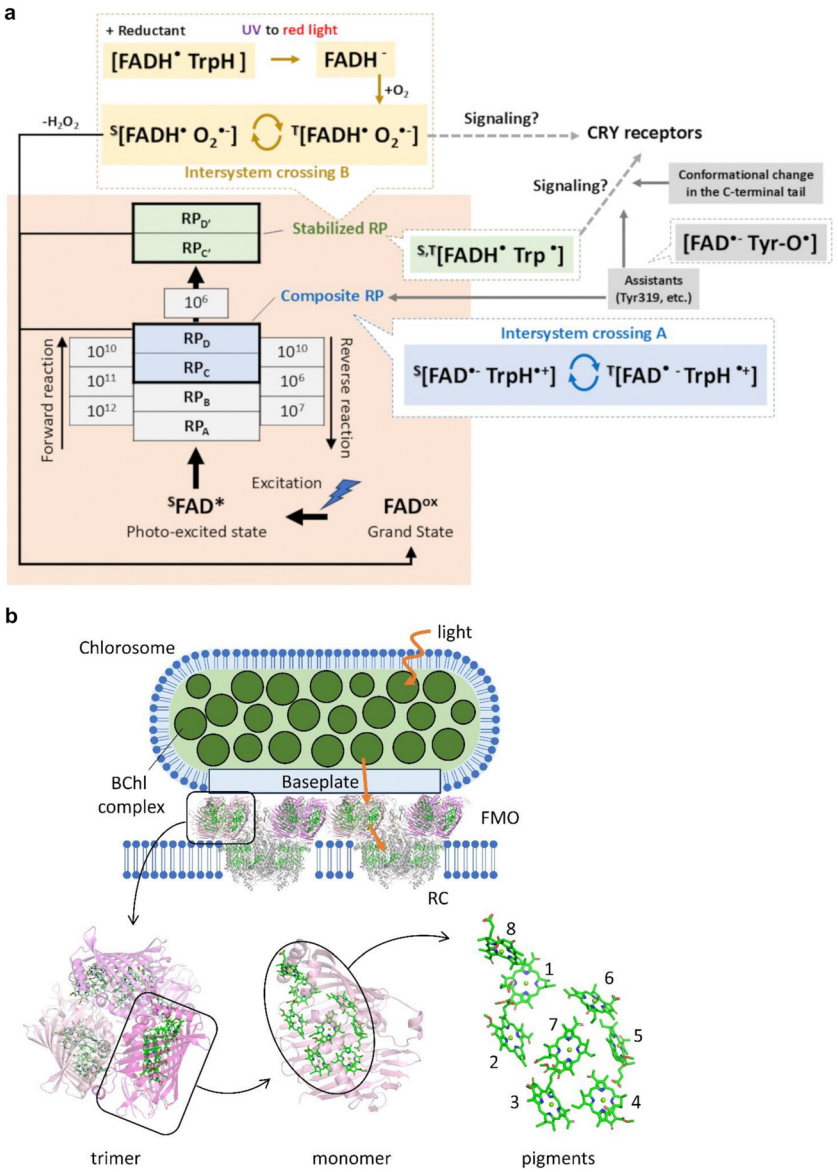

Fig. 9 Reaction scheme of avian CRY4 and light-harvesting system in green sulfur bacteria. (a) Superscripts S and T indicate singlet and triplet states, respectively. The orange area shows the reaction scheme determined from *E. rubecula* CRY4 recently.[213] The stabilized RP (green) converted from the composite RP (blue) would trigger the signaling. The curve arrows indicate the coherent, magnetic field-dependent intersystem crossing. The broken arrows indicate the unknown processes. The magnetic signaling could be proceeded by the assistance from Tyr319 and/or the conformational change in the C-terminal tail (grey).[216,217,230] Another process (yellow) was also proposed.[225,227,234] The CRY receptors have not yet been identified, but many candidates have been proposed.[221,235–238] (b) Chlorosomes contain 100 000–200 000 BChl *c* molecules, and self-aggregated BChls are packed inside a lipid envelope. The chlorosome protein CmsA forms the oligomeric BChl *a*-CmsA complexes in the chlorosome envelope called baseplate. Homotrimers of the FMO proteins associate with the baseplate of chlorosome. The FMO proteins connect the chlorosome with the RCs embedded in the cytoplasmic membrane. The structural models for the FMO-RC complex (PDB ID: 7Z6Q)[239] and the FMO protein (PDB ID: 3ENI)[240] are shown as ribbons for protein moieties and sticks for pigments. Fig. 9a was reproduced from Fig. 4a from ref. 213 with permission form Springer Nature, copyright 2024.

of CRY-based magnetoreception, many mysteries remain, including how sensed magnetic information is propagated to the brain and contributes to decision-making for the direction.

4.4. Light-dependent reactions in photosynthesis

Photosynthesis is the fundamental biological process of converting light into chemical energy, essential for living organisms. Photosynthetic organisms are classified into the oxygenic and anoxygenic types. The former is observed in higher plants, algae, and cyanobacteria, and the latter in green sulfur and purple bacteria. Photosynthesis for both types consists of two separate processes: the light-dependent reactions and the carbon fixation reactions. In higher plants, the light-dependent reactions are conducted through pigment–protein complexes embedded in thylakoid membranes inside chloroplasts.[255] The light-dependent reactions start with the capture of sunlight, which is mainly performed by light-harvesting complexes (LHC I & II), and excitation energy by sunlight is transferred to the

Open Access Article. Published on 28 Januarie 2025. Downloaded on 2026-01-31 2:57:56 nm.
This article is licensed under a Creative Commons Attribution-NonCommercial 3.0 Unported Licence.

reaction centers (RC) of photosystems (PS I & II).[256] The energy transfer process from LHCs to the RCs achieves high quantum efficiency.[257,258] The excitation energy, transferred from LHC, is absorbed by chlorophyll (Chl) molecules bound with the RC, and an electronically excited state of Chls results in a charge-separated state.[259,260] Sequential electron transfer steps stabilize the charge-separated state *via* the cofactors in the RC. The light-induced electron transfer leads to the linear electron transfer and the proton transfer driven by the four membrane protein complexes, PS II, cytochrome b_6f, PS I, and ATP synthase. Finally, the light-dependent reactions produce the energy-carrying molecule ATP and the reducing-power NADPH, and they are utilized in the subsequent carbon fixation reactions where carbon dioxides (CO_2) are converted to carbohydrates.

In oxygenic photosynthesis, PS II is the center of water oxidation, which produces dioxygen (O_2) at the oxygen-evolving complex (OEC). The water oxidation cycle contains electron and proton removing steps during four light absorption events.[261] A high-resolution X-ray crystal structure of PS II has made significant progress in understanding the water-splitting mechanism.[262] The three-dimensional structure clarified the atomic arrangement of OEC as the Mn_4CaO_5 cluster. However, later theoretical works demonstrated that the Mn_4CaO_5 complex was a mixture of oxidation states because of photoreduction by exposure to intense X-rays of synchrotron.[263,264] Recent advances in X-ray free-electron lasers (XFEL) enable solving the structure with less X-ray damage using femtosecond (fs) pulsed X-rays,[265] and various states of the catalytic cycle in water oxidation have been determined by a pump–probe method using an optical laser in combination with XFEL.[266,267] Based on the structural information, the electronic structure of the Mn_4CaO_5 complex has been studied by spectroscopic analyses and quantum chemical calculations to understand the catalytic process of water oxidation.[268]

4.5. Energy transfer in the light-harvesting system in photoreception

The absorption of sunlight by pigment molecules in light-harvesting systems causes electronic excitation states of the pigments, and then the excitation energy is efficiently funneled to the RC. Förster's theory describes the excitation energy transfer in which the coulombic interaction mediates the energy transfer between spatially separated pigments, and the excitation energy incoherently hops through adjacent pigment molecules.[269] In photosynthetic light-harvesting systems, the pigment molecules are densely assembled in protein scaffolds, and electronic solid coupling between pigments results in a delocalized excitation state among pigments.[270] The Redfield theory showed that extensive electronic coupling causes excitation relaxation.[271] The delocalized states in light-harvesting systems were positioned in the intermediate regime between weak (Förster's case) and large (Redfield's case) electronic coupling, implying that quantum coherence might participate in efficient energy transfers.[271,272] A direct observation of quantum coherence of electronic excitation states in the Fenna–Matthews–Olson (FMO) protein, the light-harvesting complex of green sulfur bacteria, was reported by Engel *et al.*[273] Their 2D spectroscopic analysis at the cryogenic temperature (77 K) demonstrated long-lived "quantum beating" for >600 fs that was longer than the dephasing timescale of electronic coherence in the FMO protein predicted by theoretical studies.[274] Since then, many spectroscopic and theoretical works have been reported to investigate whether quantum coherences contribute to efficient energy transfers by light-harvesting systems.[271,275–277] In particular, the high-speed 2D electronic spectrometer has become an invaluable tool because it can capture ultrafast coherent and non-coherent processes with high temporal and spectral resolution, allowing us to observe quantum effects occurring in complex biological systems with multiple chromophores or energy transfer pathways. When combined with molecular beam techniques, 2D electronic spectroscopy can study biological molecules with minimal environmental perturbations, allowing for the observation of intrinsic quantum effects.[278] The spectrometers disentangle vibrational coherence by resolving both excitation and detection frequencies. Cross-peaks of the 2D spectra can provide information about coupling between different energy levels, enabling us to identify vibrational coherences. In addition, measuring the 2D spectra over time also provides a dephasing time for each of the coherences.[279] Thus, the high-speed 2D electronic spectrometer has unique advantages for studying quantum effects in biological systems, such as energy transfer pathways and coherent dynamics that may be responsible for the high efficiency of specific processes and observation of intrinsic quantum effects. However, many challenges remain in understanding 2D electron spectra. It is still difficult to interpret the origins of spectra because they can contain contributions from multiple chromophores and energy transfer processes. Collecting data on specimens that differ slightly, for instance, the environment or the number of chromophores, will help us develop analysis methods and build theoretical frameworks, finally understanding quantum effects in biomolecules.

Green sulfur bacteria have large light-harvesting antennae called chlorosomes (Fig. 9b).[280] The light energy absorbed by bacteriochlorophyll (BChl) molecules in chlorosomes is transferred to the RCs *via* the FMO proteins. The FMO proteins form a homotrimer, and each monomer contains eight BChl molecules with a specific geometrical arrangement.[240] The eight BChls showed partially delocalized excitation states,[240,281] and spectroscopic data suggested that the BChl 3 is the linker pigment between the FMO protein and the RC.[240] The three-dimensional structures of the FMO-RC complex by cryo-electron microscopy (cryo-EM) revealed that the two BChls 3 in each FMO trimer are located close to the RC.[239,282,283] Suppose quantum coherence plays a role in efficient excitation energy transfer in photosynthetic apparatus. In that case, coherence must also be present at physiological temperatures, even if thermal vibrations in the protein bath accelerate decoherence. The FMO protein showed that long-lived quantum coherence was preserved even at physiological temperature (277 K).[284] Correlated motions within protein environments were thought to assist the preservation of long-lived quantum coherence in the pigment–protein complexes.[285,286] Spectroscopic and theoretical studies have suggested how quantum

 This journal is © The Royal Society of Chemistry 2025

Open Access Article. Published on 28 Januarie 2025. Downloaded on 2026-01-31 2:57:56 nm.
This article is licensed under a Creative Commons Attribution-NonCommercial 3.0 Unported Licence.

coherence influences efficient energy transfers that vibronic coupling, the interaction between electronic and nuclear vibrational motion, drives excitation energy transfers in photosynthesis.[287,288]

The interpretation of quantum coherence in photosynthesis has raised considerable debate.[275–277] Spectroscopic analyses of some groups demonstrated that the dephasing of electronic coherences in the FMO protein progressed faster than that observed in the previous study.[275,289,290] Their works suggested that the observed long-lived beating derives from vibrational modes on the electronic ground state.[275] Further experimental and theoretical studies will continue to prove the involvement of coherences in photosynthetic energy transfers. Spectroscopic and theoretical studies become necessary to deal with larger molecular assemblies, such as light-harvesting and RC complexes. Three-dimensional structural information of the complexes would greatly help these studies, and several structures have been determined for the complexes, including PS II-LHC II and PS I-LHC I, by X-ray crystallography and cryo-EM.[239,283,291–293] However, it has been reported that high-dose electron beams in cryo-EM caused damage (structural changes) in protein samples.[294] Therefore, intact structural information is needed to understand the role of coherences.

4.6. Proton tunnelling and enzyme reaction

In 1944, Schrödinger postulated a significant role for hydrogen (nuclear) tunnelling in biological reactions in *What is Life?*[295] He introduced the concept of C–H bond activation, which entails the movement of the nucleus as a wave through the reaction barrier. A notable biological process that involves C–H bond cleavage, essential for life, is the metabolism of molecules like glucose. In the 1980s, researchers began to explore the contribution of hydrogen tunnelling to enzyme reactions by measuring kinetic hydrogen isotope effects (KIEs). They incorporated hydrogen isotopes, such as deuterium (D), into stable, non-exchanging positions within samples to study the isotopic effects in enzyme-mediated reactions.

KIEs are observed in many enzymes, including soybean lipoxygenase (SLO), a paradigmatic example of quantum mechanical tunnelling in biological C–H bond cleavage reactions.[296] SLO catalyzes the production of fatty acid hydroperoxides from (*Z*,*Z*)-1,4-pentadienoic moieties through a rate-limiting proton-coupled electron transfer (net hydrogen atom transfer) from the reactive carbon (C11) of the substrate to an $Fe^{III}(OH)$ cofactor. The oxygenated lipids and their by-products produced by this reaction are essential for signalling structural and metabolic changes within the cell, contributing to processes such as seed growth and plant development.

KIEs can be classified into two distinct types: semi-classical and full tunnelling or wave function overlap regimes. In the semi-classical regime, the activation energy varies for different isotopes due to changes in the ground state energy resulting from the isotope effect. Conversely, in the tunnelling or wave function overlap regime, the activation energy remains consistent across all isotopes, attributed to the minimal distance over the energy barrier required for tunnelling. This critical distance, the hydrogen donor–acceptor distance (DAD), is theoretically calculated to range between 2.7 to 2.8 Å. In SLO, DAD has been empirically measured using electron–nuclear double resonance (ENDOR) spectroscopy.[297] Changes in DAD have been correlated with variations in activation energy caused by amino acid mutations.[298]

Temperature-dependent hydrogen–deuterium exchange coupled to mass spectrometry (TDHDX-MS) has recently been recognized as a widely accessible and practical experimental method for investigating heat-induced changes in local protein flexibility. TDHDX-MS provides a time-averaged spatial resolution of activated networks extending from protein–solvent interfaces to enzyme-active sites when combined with function-altering protein mutations. This approach has identified local networks within SLO that correlate with the activation energy for hydrogen–deuterium exchange and the enthalpic barrier for catalytic C–H bond cleavage.[299–303] Recent studies have also established a connection between the catalytic reaction and a nanosecond stoke shift observed in SLO, enhancing our understanding of the molecular mechanisms at the solvent interface.[304]

4.7. Proton tunnelling and mutation in DNA

Spontaneous mutations can arise from tautomeric shifts in nucleotide bases, a phenomenon first proposed by Watson and Crick. These shifts can lead to mismatched base pairing during DNA replication and translation.[305] Later hypotheses suggested that proton tunnelling could significantly increase the formation of rare tautomeric enol forms, leading to mismatches in nucleobase interstrand pairing and potential errors during DNA replication.[306] These mismatches, which mimic the geometry of correct Watson–Crick base pairs, are challenging to detect due to subtle chemical shifts, such as the movement of a single proton and a π-bond. Current structure determination methods like X-ray crystallography and cryo-EM analysis struggle to visualize these mismatches since protons are generally invisible by these techniques.[307] However, by integrating NMR relaxation dispersion with misincorporation rate measurements, researchers have mapped a kinetic network involving two tautomeric and one anionic Watson–Crick-like mismatches.[308] This research underscores the complexity of replication fidelity and the challenges in pinpointing the sources of errors that could lead to mutations and, potentially, cause cancer.[309]

Hydrogen transfer in DNA bases can produce transient, biologically relevant mutagens called tautomers. Keto–enol and amino–imino tautomerism are implicated in the spontaneous DNA mutation during replication and repair processes. The energy landscapes of both canonical (amino–keto) and tautomeric (imino–enol) forms of adenine–thymine (A–T) and guanine–cytosine (G–C) monomers and base pairs have been modeled using the *ab initio* quantum mechanical approach of density functional theory (DFT).[310] Understanding the time scale of these processes is crucial for comprehending the role of proton tunnelling in DNA mutation. Previous research has indicated that the lifetime of tautomers is shorter than the timescale for helicase cleavage.[311,312] Using the open quantum system (OQS) approach, where the quantum system (the H-bond proton in the double-well potential) undergoes dissipation and

Open Access Article. Published on 28 Januarie 2025. Downloaded on 2026-01-31 2:57:56 nm.. This article is licensed under a Creative Commons Attribution-NonCommercial 3.0 Unported Licence.

decoherence due to its coupling with a surrounding heat bath, it is suggested that tautomers could reach equilibrium concentration.[313] These studies propose that proton transfer through quantum tunneling can occur within a few hundred femtoseconds, potentially leading to mismatches during DNA replication. Experimental tests using neutron scattering, which can directly observe hydrogen/deuterium atoms,[314] are essential for advancing our understanding of this mechanism.

5. Conclusion

Quantum life science is still in its infancy, but it will provide new perspectives and contribute to resolving many biological phenomena that cannot be described and understood by conventional molecular mechanics or molecular biology. However, observing the quantum effect in living organisms is still challenging because it is very subtle, quickly dissipates, and gets decoherent under physiological conditions. To overcome the problems, it is essential to develop quantum sensors with more NV centers in nanodiamonds and hyperpolarized MRI/NMR molecules for higher accuracy. Moreover, new device development, such as two-dimensional electronic spectroscopy using a high-speed and stable 2D electronic spectrometer that can disentangle the vibrational coherence,[315] helps deepen our understanding of the role of quantum effects in living systems. Such technologies and knowledge bring about the development of novel devices that utilize or mimic biological systems like photosynthesis, magnetoreception, and so on. It is strongly expected that the development of Quantum Life Sciences will elucidate a series of life phenomena that could not be elucidated by molecular biology and bring about innovative technological innovations that mimic these phenomena.

Through further quantum life science research in the future, we will contribute to the development of a paradigm shift in life science, as well as the development of new cancer diagnosis and treatment methods, contributions to regenerative medicine, elucidation of brain function, elucidation of the aging process, and other innovations in the medical and healthcare fields. In addition, we will contribute to developing a peaceful and fulfilling human society by bringing about innovations in information, energy, agriculture, the environment, and space. However, quantum life science is a new academic discipline, and few researchers specialize in this field, so growing young researchers and experts is an extremely important issue. For this reason, establishing and improving specialized courses to teach quantum life science at universities and research institutions will be extremely important in the future.

Author contributions

Y. B. conceived the idea. Y. B., H. Y., and H. K. designed and decided the outline of this paper. H. Y., H. K., H. I., R. I., Y. T., S. A., and Y. H. conducted the literature study, interpreted the collected data, drew the figures, and wrote the manuscript. All authors checked and approved the manuscript and figures.

Data availability

No primary research results, software or code have been included and no new data were generated or analysed as part of this review.

Conflicts of interest

The authors declare no conflicts of interest.

Acknowledgements

This paper was supported by the MEXT Quantum Leap Flagship Program (MEXT Q-LEAP, JPMXS0120330644).

References

1 L. Slocombe, M. Sacchi and J. Al-Khalili, *Commun. Phys.*, 2022, **5**, 109.
2 C. L. Degen, F. Reinhard and P. Cappellaro, *Rev. Mod. Phys.*, 2017, **89**, 035002.
3 D. Budker and M. Romalis, *Nat. Phys.*, 2007, **3**, 227–234.
4 J. F. Barry, J. M. Schloss, E. Bauch, M. J. Turner, C. A. Hart, L. M. Pham and R. L. Walsworth, *Rev. Mod. Phys.*, 2020, **92**, 015004.
5 R. Schirhagl, K. Chang, M. Loretz and C. L. Degen, *Annu. Rev. Phys. Chem.*, 2014, **65**, 83–105.
6 M. Simmonds, W. Fertig and R. Giffard, *IEEE Trans. Magn.*, 1979, **15**, 478–481.
7 H. B. Dang, A. C. Maloof and M. V. Romalis, *Appl. Phys. Lett.*, 2010, **397**, 151110.
8 M. Brownnutt, M. Kumph, P. Rabl and R. Blatt, *Rev. Mod. Phys.*, 2015, **87**(4), 1419.
9 G. Balasubramanian, I. Y. Chan, R. Kolesov, M. Al-Hmoud, J. Tisler, C. Shin, C. Kim, A. Wojcik, P. R. Hemmer, A. Krueger, T. Hanke, A. Leitenstorfer, R. Bratschitsch, F. Jelezko and J. Wrachtrup, *Nature*, 2008, **455**, 648–651.
10 J. R. Maze, P. L. Stanwix, J. S. Hodges, S. Hong, J. M. Taylor, P. Cappellaro, L. Jiang, M. V. Gurudev Dutt, E. Togan, A. S. Zibrov, A. Yacoby, R. L. Walsworth and M. D. Lukin, *Nature*, 2008, **455**, 644–647.
11 A. M. Zaitsev, *Phys. Rev. B: Condens. Matter Mater. Phys.*, 2000, **61**, 12909.
12 S. Castelletto and A. Boretti, *J. Phys. Photonics*, 2020, **2**, 022001.
13 A. R.-P. Montblanch, M. Barbone, I. Aharonovich, M. Atatüre and A. C. Ferrari, *Nat. Nanotechnol.*, 2023, **18**, 555–571.
14 S. G. Bishop, J. P. Hadden, F. D. Alzahrani, R. Hekmati, D. L. Huffaker, W. W. Langbein and A. J. Bennett, *ACS Photonics*, 2020, **7**, 1636.
15 A. M. Berhane, K.-Y. Jeong, Z. Bodrog, S. Fiedler, T. Schröder, N. V. Triviño, T. Palacios, A. Gali, M. Toth, D. Englund and I. Aharonovich, *Adv. Mater.*, 2017, **29**, 1605092.
16 P. Reineck, A. Francis, A. Orth, D. W. M. Lau, R. D. V. Nixon-Luke, I. D. Rastogi, W. A. W. Razali, N. M. Cordina, L. M. Parker, V. K. A. Sreenivasan, L. J. Brown and B. C. Gibson, *Adv. Opt. Mater.*, 2016, **4**, 1549.

 This journal is © The Royal Society of Chemistry 2025

Open Access Article. Published on 28 Januarie 2025. Downloaded on 2026-01-31 2:57:56 nm.
This article is licensed under a Creative Commons Attribution-NonCommercial 3.0 Unported Licence.

17 A. Gruber, A. Dräbenstedt, C. Tietz, L. Fleury, J. Wrachtrup and C. von Borczyskowski, *Science*, 1997, **276**, 2012–2014.
18 D. Terada, T. F. Segawa, A. I. Shames, S. Onoda, T. Ohshima, E. Ōsawa, R. Igarashi and M. Shirakawa, *ACS Nano*, 2019, **13**, 6461.
19 L. Nie, A. C. Nusantara, V. G. Damle, R. Sharmin, E. P. P. Evans, S. R. Hemelaar, K. J. van der Laan, R. Li, F. P. P. Martinez, T. Vedelaar, M. Chipaux and R. Schirhagl, *Sci. Adv.*, 2021, **7**, 573.
20 R. Igarashi, T. Sugi, S. Sotoma, T. Genjo, Y. Kumiya, E. Walinda, H. Ueno, K. Ikeda, H. Sumiya, H. Tochio, Y. Yoshinari, Y. Harada and M. Shirakawa, *J. Am. Chem. Soc.*, 2020, **142**, 7542–7554.
21 M. Fujiwara, S. Sun, A. Dohms, Y. Nishimura, K. Suto, Y. Takezawa, K. Oshimi, L. Zhao, N. Sadzak, Y. Umehara, Y. Teki, N. Komatsu, O. Benson, Y. Shikano and E. Kage-Nakadai, *Sci. Adv.*, 2020, **6**, eaba9636.
22 I. Lovchinsky, A. O. Sushkov, E. Urbach, N. P. de Leon, S. Choi, K. De Greve, R. Evans, R. Gertner, E. Bersin, C. Müller, L. McGuinness, F. Jelezko, R. L. Walsworth, H. Park and M. D. Lukin, *Science*, 2016, **351**, 836.
23 F. Shi, Q. Zhang, P. Wang, H. Sun, J. Wang, X. Rong, M. Chen, C. Ju, F. Reinhard, H. Chen, J. Wrachtrup, J. Wang and J. Du, *Science*, 2015, **347**, 1135–1138.
24 C. Zhang, F. Shagieva, M. Widmann, M. Kübler, V. Vorobyov, P. Kapitanova, E. Nenasheva, R. Corkill, O. Rhrle, K. Nakamura, H. Sumiya, S. Onoda, J. Isoya and J. Wrachtrup, *Phys. Rev. Appl.*, 2021, **15**, 064075.
25 F. Dolde, H. Fedder, M. W. Doherty, T. Nöbauer, F. Rempp, G. Balasubramanian, T. Wolf, F. Reinhard, L. C. L. Hollenberg, F. Jelezko and J. Wrachtrup, *Nat. Phys.*, 2011, **7**, 459–463.
26 G. Kucsko, P. C. Maurer, N. Y. Yao, M. Kubo, H. J. Noh, P. K. Lo, H. Park and M. D. Lukin, *Nature*, 2013, **500**, 54–58.
27 S. Hsieh, P. Bhattacharyya, C. Zu, T. Mittiga, T. J. Smart, F. Machado, B. Kobrin, T. O. Höhn, N. Z. Rui, M. Kamrani, S. Chatterjee, S. Choi, M. Zaletel, V. V. Struzhkin, J. E. Moore, V. I. Levitas, R. Jeanloz and N. Y. Yao, *Science*, 2019, **366**, 1349–1354.
28 T. Staudacher, N. Raatz, S. Pezzagna, J. Meijer, F. Reinhard, C. A. Meriles and J. Wrachtrup, *Nat. Commun.*, 2015, **6**, 8527.
29 H. Ishiwata, H. C. Watanabe, S. Hanashima, T. Iwasaki and M. Hatano, *Adv. Quantum Technol.*, 2021, **4**(4), 2000106.
30 T. Wolf, P. Neumann, K. Nakamura, H. Sumiya, T. Ohshima, J. Isoya and J. Wrachtrup, *Phys. Rev. X*, 2015, **5**, 041001.
31 J. M. Taylor, P. Cappellaro, L. Childress, L. Jiang, D. Budker, P. R. Hemmer, A. Yacoby, R. Walsworth and M. D. Lukin, *Nat. Phys.*, 2008, **4**(10), 810.
32 P. K. Bachmann, D. Leers and H. Lydtin, *Diamond Relat. Mater.*, 1991, **1**(1), 1.
33 Y. N. Palyanov, Y. M. Borzdov, A. F. Khokhryakov, I. N. Kupriyanov and A. G. Sokol, *Cryst. Growth Des.*, 2010, **10**(7), 3169.
34 E. Six, The Element Six CVD Diamond Handbook, **https://e6cvd.com/media/wysiwyg/pdf/E6_CVD_Diamond_Handbook_A5_v10X.pdf**.
35 T. Teraji, T. Yamamoto, K. Watanabe, Y. Koide, J. Isoya, S. Onoda, T. Ohshima, L. J. Rogers, F. Jelezko, P. Neumann, J. Wrachtrup and S. Koizumi, *Phys. Status Solidi A*, 2015, **212**(11), 2365.
36 G. Balasubramanian, P. Neumann, D. Twitchen, M. Markham, R. Kolesov, N. Mizuochi, J. Isoya, J. Achard, J. Beck, J. Tissler, V. Jacques, P. R. Hemmer, F. Jelezko and J. Wrachtrup, *Nat. Mater.*, 2009, **8**, 383–387.
37 V. N. Mochalin, O. Shenderova, D. Ho and Y. Gogotsi, *Nat. Nanotechnol.*, 2012, **7**, 11.
38 O. A. Shenderova, A. I. Shames, N. A. Nunn, M. D. Torelli, I. Vlasov and A. Zaitsev, *J. Vac. Sci. Technol., B: Nanotechnol. Microelectron.: Mater., Process., Meas., Phenom.*, 2019, **37**, 030802.
39 M. Fujiwara and Y. Shikano, *Nanotechnology*, 2021, **32**, 482002.
40 A. Haque and S. Sumaiya, *J. Manuf. Mater. Process*, 2017, **1**(1), 6.
41 V. M. Acosta, E. Bauch, M. P. Ledbetter, C. Santori, K.-M. C. Fu, P. E. Barclay, R. G. Beausoleil, H. Linget, J. F. Roch, F. Treussart, S. Chemerisov, W. Gawlik and D. Budker, *Phys. Rev. B: Condens. Matter Mater. Phys.*, 2009, **80**, 115202.
42 S. Sangtawesin, T. O. Brundage, Z. J. Atkins and J. R. Petta, *Appl. Phys. Lett.*, 2014, **105**, 063107.
43 L. M. Pham, S. J. DeVience, F. Casola, I. Lovchinsky, A. O. Sushkov, E. Bersin, J. Lee, E. Urbach, P. Cappellaro, H. Park, A. Yacoby, M. Lukin and R. L. Walsworth, *Phys. Rev. B*, 2016, **93**, 04542.
44 D. M. Toyli, C. D. Weis, G. D. Fuchs, T. Schenkel and D. D. Awschalom, *Nano Lett.*, 2010, **10**(8), 3168.
45 A. Sipahigil, R. E. Evans, D. D. Sukachev, M. J. Burek, J. Borregaard, M. K. Bhaskar, C. T. Nguyen, J. L. Pacheco, H. A. Atikian, C. Meuwly, R. M. Camacho, F. Jelezko, E. Bielejec, H. Park, M. Lončar and M. D. Lukin, *Science*, 2016, **354**(6314), 847.
46 S. Pezzagna, D. Wildanger, P. Mazarov, A. D. Wieck, Y. Sarov, I. Rangelow, B. Naydenov, F. Jelezko, S. W. Hell and J. Meijer, *Small*, 2010, **6**(19), 2117.
47 T. Luhmann, N. Raatz, R. John, M. Lesik, J. Rodiger, M. Portail, D. Wildanger, F. Kleißler, K. Nordlund, A. Zaitsev, J. F. Roch, A. Tallaire, J. Meijer and S. Pezzagna, *J. Phys. D: Appl. Phys.*, 2018, **51**(48), 483002.
48 Y. C. Chen, B. Griffiths, L. Weng, S. S. Nicley, S. N. Ishmael, Y. Lekhai, S. Johnson, C. J. Stephen, B. L. Green, G. W. Morley, M. E. Newton, M. J. Booth, P. S. Salter and J. M. Smith, *Optica*, 2019, **6**(5), 662.
49 D. R. Glenn, D. B. Bucher, J. Lee, M. D. Lukin, H. Park and R. L. Walsworth, *Nature*, 2018, **555**, 351.
50 L. B. Hughes, Z. Zhang, C. Jin, S. A. Meynell, B. Ye, W. Wu, Z. Wang, E. J. Davis, T. E. Mates, N. Y. Yao, K. Mukherjee and A. C. Bleszynski Jayich, *APL Mater.*, 2023, **11**, 021101.
51 K. Ohno, F. J. Heremans, L. C. Bassett, B. A. Myers, D. M. Toyli, A. C. Bleszynski Jayich, C. J. Palmstrøm and D. D. Awschalom, *Appl. Phys. Lett.*, 2012, **101**(8), 082413.
52 T. Fukui, Y. Doi, T. Miyazaki, Y. Miyamoto, H. Kato, T. Matsumoto, T. Makino, S. Yamasaki, R. Morimoto, N. Tokuda, M. Hatano, Y. Sakagawa, H. Morishita,

Open Access Article. Published on 28 Januarie 2025. Downloaded on 2026-01-31 2:57:56 nm.
This article is licensed under a Creative Commons Attribution-NonCommercial 3.0 Unported Licence.

T. Tashima, S. Miwa, Y. Suzuki and N. Mizuochi, *Appl. Phys. Express*, 2014, **7**, 055201.
53 T. Miyazaki, R. Miyamoto, T. Makino, H. Kato, S. Yamasaki, T. Fukui, Y. Doi, N. Tokuda, M. Hatano and N. Mizuochi, *Appl. Phys. Lett.*, 2014, **105**, 261601.
54 H. Ozawa, K. Tahara, H. Ishiwata, M. Hatano and T. Iwasaki, *Appl. Phys. Express*, 2017, **10**, 04550.
55 H. Ishiwata, M. Nakajima, K. Tahara, H. Ozawa, T. Iwasaki and M. Hatano, *Appl. Phys. Lett.*, 2017, **111**, 04310.
56 T. Tsuji, T. Iwasaki and M. Hatano, *Appl. Phys. Express*, 2023, **16**, 025503.
57 R. Kawase, H. Kawashima, H. Kato, N. Tokuda, S. Yamasaki, M. Ogura, T. Makino and N. Mizuochi, *J. Appl. Phys.*, 2022, **132**, 174504.
58 E. D. Herbschleb, H. Kato, T. Makino, S. Yamasaki and N. Mizuochi, *Nat. Commun.*, 2021, **12**, 306.
59 N. R. Greiner, D. S. Phillips, J. D. Johnson and F. Volk, *Nature*, 1988, **333**, 440.
60 J.-P. Boudou, P. A. Curmi, F. Jelezko, J. Wrachtrup, P. Aubert, M. Sennour, G. Balasubramanian, R. Reuter, A. Thorel and E. Gaffet, *Nanotechnology*, 2009, **20**, 235602.
61 A. K. Khachatryan, S. G. Aloyan, P. W. May, R. Sargsyan, V. A. Khachatryan and V. S. Baghdasaryan, *Diamond Relat. Mater.*, 2008, **17**, 931.
62 D. Amans, M. Diouf, J. Lam, G. Ledoux and C. Dujardin, *J. Colloid Interface Sci.*, 2017, **489**, 114.
63 M. E. Trusheim, L. Li, A. Laraoui, E. H. Chen, H. Bakhru, T. Schröder, O. Gaathon, C. A. Meriles and D. Englund, *Nano Lett.*, 2013, **14**, 32.
64 J. Tisler, G. Balasubramanian, B. Naydenov, R. Kolesov, B. Grotz, R. Reuter, J. P. Boudou, P. A. Curmi, M. Sennour, A. Thorel, M. Börsch, K. Aulenbacher, R. Erdmann, P. R. Hemmer, F. Jelezko and J. Wrachtrup, *ACS Nano*, 2009, **3**, 1959.
65 F. T.-K. So, A. I. Shames, D. Terada, T. Genjo, H. Morishita, I. Ohki, T. Ohshima, S. Onoda, H. Takashima, S. Takeuchi, N. Mizuochi, R. Igarashi, M. Shirakawa and T. F. Segawa, *J. Phys. Chem. C*, 2022, **126**, 5206.
66 C. Bradac, T. Gaebel, N. Naidoo, M. J. Sellars, J. Twamley, L. J. Brown, A. S. Barnard, T. Plakhotnik, A. V. Zvyagin and J. R. Rabeau, *Nat. Nanotechnol.*, 2010, **5**, 345–349.
67 S. Kumar, M. Nehra, D. Kedia, N. Dilbaghi, K. Tankeshwar and K. H. Kim, *Carbon*, 2019, **143**, 678.
68 O. A. Shenderova and G. E. McGuire, *Biointerphases*, 2015, **10**, 030802.
69 R. H. Wentorf, *J. Phys. Chem.*, 1965, **69**, 3063.
70 E. A. Ekimov, O. S. Kudryavtsev, N. E. Mordvinova, O. I. Lebedev and I. I. Vlasov, *ChemNanoMat*, 2018, **4**, 269.
71 M. A. Gebbie, H. Ishiwata, P. J. McQuade, V. Petrak, A. Taylor, C. Freiwald, J. E. Dahl, R. M. K. Carlson, A. A. Fokin, P. R. Schreiner, Z. X. Shen, M. Nesladek and N. A. Melosh, *Proc. Natl. Acad. Sci. U. S. A.*, 2018, **115**(33), 8284–8289.
72 K. Oshimi, H. Nakashima, S. Mandić, H. Kobayashi, M. Teramoto, H. Tsuji, Y. Nishibayashi, Y. Shikano, T. An and M. Fujiwara, *ACS Nano*, 2024, **18**(52), 35202–35313.
73 F. Maier, M. Riedel, B. Mantel, J. Ristein and L. Ley, *Phys. Rev. Lett.*, 2000, **85**, 3472.
74 S. Kawai, H. Yamano, T. Sonoda, K. Kato, J. J. Buendia, T. Kageura, R. Fukuda, T. Okada, T. Tanii, T. Higuchi, M. Haruyama, K. Yamada, S. Onoda, T. Ohshima, W. Kada, O. Hanaizumi, A. Stacey, T. Teraji, S. Kono, J. Isoya and H. Kawarada, *J. Phys. Chem. C*, 2019, **123**(6), 3594–3604.
75 B. A. Myers, A. Das, M. C. Dartiailh, K. Ohno, D. D. Awschalom and A. C. B. Jayich, *Phys. Rev. Lett.*, 2014, **113**, 027602.
76 S. Sangtawesin, B. L. Dwyer, S. Srinivasan, J. J. Allred, L. V. H. Rodgers, K. De Greve, A. Stacey, N. Dontschuk, K. M. O'Donnell, D. Hu, D. A. Evans, C. Jaye, D. A. Fischer, M. L. Markham, D. J. Twitchen, H. Park, M. D. Lukin and N. P. de Leon, *Phys. Rev. X*, 2019, **9**(3), 031052.
77 Y. V. Butenko, V. L. Kuznetsov, E. A. Paukshtis, A. I. Stadnichenko, I. N. Mazov, S. I. Moseenkov, A. I. Boronin and S. V. Kosheev, *Fullerenes, Nanotubes, Carbon Nanostruct.*, 2006, **14**, 557.
78 V. Pichot, M. Comet, E. Fousson, C. Baras, A. Senger, F. Le Normand and D. Spitzer, *Diamond Relat. Mater.*, 2008, **17**, 13.
79 S. Osswald, G. Yushin, V. Mochalin, S. O. Kucheyev and Y. Gogotsi, *J. Am. Chem. Soc.*, 2006, **128**, 11635.
80 K. S. Liu, A. Henning, M. W. Heindl, R. D. Allert, J. D. Bart, I. D. Sharp, R. Rizzato and D. B. Bucher, *Proc. Natl. Acad. Sci. U. S. A.*, 2022, **119**(5), e2111607119.
81 J. M. Abendroth, K. Herb, E. Janitz, T. Zhu, L. A. Völker and C. L. Degen, *Nano Lett.*, 2022, **22**, 7294–7303.
82 M. Xie, X. Yu, L. V. H. Rodgers, D. Xu, I. Chi-Duran, A. Toros, N. Quack, N. P. de Leon and P. C. Maurer, *Proc. Natl. Acad. Sci. U. S. A.*, 2022, **119**(8), e2114186119.
83 Y. Wu and T. Weil, *Adv. Sci.*, 2022, **9**, 2200059.
84 F. Jelezko and J. Wrachtrup, *Phys. Status Solidi A*, 2006, **203**, 3207–3225.
85 G. Thiering and A. Gali, *Phys. Rev. B: Condens. Matter Mater. Phys.*, 2018, **98**, 085207.
86 A. T. Collins, M. F. Thomaz and M. I. B. Jorge, *J. Phys. C: Solid State Phys.*, 1983, **16**, 2177.
87 S. Sotoma, C. Zhong, J. C. Y. Kah, H. Yamashita, T. Plakhotnik, Y. Harada and M. Suzuki, *Sci. Adv.*, 2021, **7**, eabd7888.
88 E. V. Levine, M. J. Turner, P. Kehayias, C. A. Hart, N. Langellier, R. Trubko, D. R. Glenn, R. R. Fu and R. L. Walsworth, *Nanophotonics*, 2019, **8**(11), 1945–1973.
89 E. Bauch, C. A. Hart, J. M. Schloss, M. J. Turner, J. F. Barry, P. Kehayias, S. Singh and R. L. Walsworth, *Phys. Rev. X*, 2018, **8**, 031025.
90 T. Rendler, J. Neburkova, O. Zemek, J. Kotek, A. Zappe, Z. Chu, P. Cigler and J. Wrachtrup, *Nat. Commun.*, 2017, **8**, 14701.
91 T. Fujisaku, R. Tanabe, S. Onoda, R. Kubota, T. F. Segawa, F. T.-K. So, T. Ohshima, I. Hamachi, M. Shirakawa and R. Igarashi, *ACS Nano*, 2019, **13**, 11726–11732.
92 T. Fujisaku, R. Igarashi and M. Shirakawa, *Chemosensors*, 2020, **8**, 68.

 This journal is © The Royal Society of Chemistry 2025

Open Access Article. Published on 28 Januarie 2025. Downloaded on 2026-01-31 2:57:56 nm.
This article is licensed under a Creative Commons Attribution-NonCommercial 3.0 Unported Licence.

93 T. F. Segawa and R. Igarashi, *Prog. Nucl. Magn. Reson. Spectrosc.*, 2023, **134–135**, 20–38.
94 V. M. Acosta, E. Bauch, M. P. Ledbetter, A. Waxman, L.-S. Bouchard and D. Budker, *Phys. Rev. Lett.*, 2010, **104**, 070801.
95 P. Neumann, I. Jakobi, F. Dolde, C. Burk, R. Reuter, G. Waldherr, J. Honert, T. Wolf, A. Brunner and J. H. Shim, *Nano Lett.*, 2013, **13**, 2738–2742.
96 P. Konzelmann, T. Rendler, V. Bergholm, A. Zappe, V. Pfannenstill, M. Garsi, F. Ziem, M. Niethammer, M. Widmann, S.-Y. Lee, P. Neumann and J. Wrachtrup, *New J. Phys.*, 2018, **20**, 123013.
97 H. J. Mamin, M. H. Sherwood, M. Kim, C. T. Rettner, K. Ohno, D. D. Awschalom and D. Rugar, *Phys. Rev. Lett.*, 2014, **113**, 030803.
98 L. T. Hall, G. C. G. Beart, E. A. Thomas, D. A. Simpson, L. P. McGuinness, J. H. Cole, J. H. Manton, R. E. Scholten, F. Jelezko, J. Wrachtrup, S. Petrou and L. C. L. Hollenberg, *Sci. Rep.*, 2012, **2**, 401.
99 A. Ermakova, G. Pramanik, J.-M. Cai, G. Algara-Siller, U. Kaiser, T. Weil, Y.-K. Tzeng, H. C. Chang, L. P. McGuinness, M. B. Plenio, B. Naydenov and F. Jelezko, *Nano Lett.*, 2013, **13**, 3305–3309.
100 J. Barton, M. Gulka, J. Tarabek, Y. Mindarava, Z. Wang, J. Schimer, H. Raabova, J. Bednar, M. B. Plenio, F. Jelezko, M. Nesladek and P. Cigler, *ACS Nano*, 2020, **14**, 12938–12950.
101 T. Yanagi, K. Kaminaga, M. Suzuki, H. Abe, H. Yamamoto, T. Ohshima, A. Kuwahata, M. Sekino, T. Imaoka, S. Kakinuma, T. Sugi, W. Kada, O. Hanaizumi and R. Igarashi, *ACS Nano*, 2021, **15**, 12869–12879.
102 M. Lobikin, B. Chernet, D. Lobo and M. Levin, *Phys. Biol.*, 2012, **9**, 065002.
103 M. Fujiwara, R. Tsukahara, Y. Sera, H. Yukawa, Y. Baba, S. Shikata and H. Hashimoto, *RSC Adv.*, 2019, **9**, 12606–12614.
104 Y. Nishimura, K. Oshimi, Y. Umehara, Y. Kumon, K. Miyaji, H. Yukawa, Y. Shikano, T. Matsubara, M. Fujiwara, Y. Baba and Y. Teki, *Sci. Rep.*, 2021, **11**, 4248.
105 K. Oshimi, Y. Nishimura, T. Matsubara, M. Tanaka, E. Shikoh, L. Zhao, Y. Zou, N. Komatsu, Y. Ikado, Y. Takezawa, E. Kage-Nakadai, Y. Izutsu, K. Yoshizato, S. Morita, M. Tokunaga, H. Yukawa, Y. Baba, Y. Teki and M. Fujiwara, *Lab Chip*, 2022, **22**, 2519–2530.
106 H. Yukawa, M. Fujiwara, K. Kobayashi, Y. Kumon, K. Miyaji, Y. Nishimura, K. Oshimi, Y. Umehara, Y. Teki, T. Iwasaki, M. Hatano, H. Hashimoto and Y. Baba, *Nanoscale Adv.*, 2020, **2**, 1859–1868.
107 L.-R. Zou, X.-D. Lyu, D.-D. Sang, Y. Yao, S.-H. Ge, X.-T. Wang, C.-D. Zhou, H.-L. Fu, H.-Z. Xi, J.-C. Fan, C. Wang and Q.-L. Wang, *Rare Met.*, 2023, **42**, 3201–3211.
108 L.-R. Zou, D.-D. Sang, Y. Yao, X.-T. Wang, Y.-Y. Zheng, N.-Z. Wang, C. Wang and Q.-L. Wang, *Rare Met.*, 2022, **42**, 17–38.
109 R. Jha, P. Mishra and S. Kumar, *Biosens. Bioelectron.*, 2024, **254**, 116232.
110 E. M. Purcell, H. C. Torrey and R. V. Pound, *Phys. Rev.*, 1946, **69**, 1–2.
111 F. Bloch, W. W. Hansen and M. Packard, *Phys. Rev.*, 1946, **70**, 7–8.
112 B. Meyer and T. Peters, *Angew. Chem., Int. Ed.*, 2003, **42**, 864–890.
113 P. Lauterbur, *Nature*, 1973, **242**, 190–191.
114 S. Mansson, E. Johansson, P. Magnusson, C. M. Chai, G. Hansson, J. S. Petersson, F. Stahlberg and K. Golman, *Eur. Radiol.*, 2006, **16**, 57–67.
115 J. Eills, D. Budker, S. Cavagnero, E. Y. Chekmenev, S. J. Elliott, S. Jannin, A. Lesage, J. Matysik, T. Meersmann, T. Prisner, J. A. Reimer, H. Yang and I. V. Koptyug, *Chem. Rev.*, 2023, **123**, 1417–1551.
116 A. W. Overhauser, *Phys. Rev.*, 1953, **92**, 411.
117 T. R. Carver and C. P. Slichter, *Phys. Rev.*, 1953, **92**, 212.
118 A. Kumar, R. R. Ernst and K. Wüthrich, *Top. Catal.*, 1980, **95**, 1–6.
119 L. R. Becerra, G. J. Gerfen, R. J. Temkin, D. J. Singel and R. G. Griffin, *Phys. Rev. Lett.*, 1993, **71**, 3561–3564.
120 A. Abragam and M. Goldman, *Rep. Prog. Phys.*, 1978, **41**, 395–467.
121 H. E. Moller, X. J. Chen, B. Saam, K. D. Hagspiel, G. A. Johnson, T. A. Altes, E. E. de Lange and H. U. Kauczor, *Magn. Reson. Med.*, 2002, **47**, 1029–1051.
122 M. S. Albert, G. D. Cates, B. Driehuys, W. Happer, B. Saam, C. S. Springer, Jr. and A. Wishnia, *Nature*, 1994, **370**, 199–201.
123 D. J. Lurie, D. M. Bussell, L. H. Bell and J. R. Mallard, *J. Magn. Reson.*, 1988, **76**, 366–370.
124 M. C. Krishna, S. English, K. Yamada, J. Yoo, R. Murugesan, N. Devasahayam, J. A. Cook, K. Golman, J. H. Ardenkjaer-Larsen, S. Subramanian and J. B. Mitchell, *Proc. Natl. Acad. Sci. U. S. A.*, 2002, **99**, 2216–2221.
125 H. Utsumi, K. Yamada, K. Ichikawa, K. Sakai, Y. Kinoshita, S. Matsumoto and M. Nagai, *Proc. Natl. Acad. Sci. U. S. A.*, 2006, **103**, 1463–1468.
126 S. Matsumoto, H. Yasui, S. Batra, Y. Kinoshita, M. Bernardo, J. P. Munasinghe, H. Utsumi, R. Choudhuri, N. Devasahayam, S. Subramanian, J. B. Mitchell and M. C. Krishna, *Proc. Natl. Acad. Sci. U. S. A.*, 2009, **106**, 17898–17903.
127 J. B. Hovener, A. N. Pravdivtsev, B. Kidd, C. R. Bowers, S. Gloggler, K. V. Kovtunov, M. Plaumann, R. Katz-Brull, K. Buckenmaier, A. Jerschow, F. Reineri, T. Theis, R. V. Shchepin, S. Wagner, P. Bhattacharya, N. M. Zacharias and E. Y. Chekmenev, *Angew. Chem., Int. Ed.*, 2018, **57**, 11140–11162.
128 J. Natterer and J. Bargon, *Prog. Nucl. Magn. Reson. Spectrosc.*, 1997, **31**, 293–315.
129 K. V. Kovtunov, E. V. Pokochueva, O. G. Salnikov, S. F. Cousin, D. Kurzbach, B. Vuichoud, S. Jannin, E. Y. Chekmenev, B. M. Goodson, D. A. Barskiy and I. V. Koptyug, *Chem. – Asian J.*, 2018, **13**, 1857–1871.
130 P. J. Rayner and S. B. Duckett, *Angew. Chem., Int. Ed.*, 2018, **57**, 6742–6753.
131 J. F. P. Colell, M. Emondts, A. W. J. Logan, K. Shen, J. Bae, R. V. Shchepin, G. X. Ortiz, Jr., P. Spannring, Q. Wang, S. J. Malcolmson, E. Y. Chekmenev, M. C. Feiters, F. Rutjes, B. Blumich, T. Theis and W. S. Warren, *J. Am. Chem. Soc.*, 2017, **139**, 7761–7767.

Open Access Article. Published on 28 Januarie 2025. Downloaded on 2026-01-31 2:57:56 nm.
This article is licensed under a Creative Commons Attribution-NonCommercial 3.0 Unported Licence.

132 R. W. Adams, J. A. Aguilar, K. D. Atkinson, M. J. Cowley, P. I. Elliott, S. B. Duckett, G. G. Green, I. G. Khazal, J. Lopez-Serrano and D. C. Williamson, *Science*, 2009, **323**, 1708–1711.
133 F. Reineri, T. Boi and S. Aime, *Nat. Commun.*, 2015, **6**, 5858.
134 J. H. Ardenkjaer-Larsen, B. Fridlund, A. Gram, G. Hansson, L. Hansson, M. H. Lerche, R. Servin, M. Thaning and K. Golman, *Proc. Natl. Acad. Sci. U. S. A.*, 2003, **100**, 10158–10163.
135 M. Vaeggemose, R. F. Schulte and C. Laustsen, *Metabolites*, 2021, **11**, 219.
136 J. H. Ardenkjaer-Larsen, *J. Magn. Reson.*, 2016, **264**, 3–12.
137 J. Kurhanewicz, D. B. Vigneron, J. H. Ardenkjaer-Larsen, J. A. Bankson, K. Brindle, C. H. Cunningham, F. A. Gallagher, K. R. Keshari, A. Kjaer, C. Laustsen, D. A. Mankoff, M. E. Merritt, S. J. Nelson, J. M. Pauly, P. Lee, S. Ronen, D. J. Tyler, S. S. Rajan, D. M. Spielman, L. Wald, X. Zhang, C. R. Malloy and R. Rizi, *Neoplasia*, 2019, **21**, 1–16.
138 Z. J. Wang, M. A. Ohliger, P. E. Z. Larson, J. W. Gordon, R. A. Bok, J. Slater, J. E. Villanueva-Meyer, C. P. Hess, J. Kurhanewicz and D. B. Vigneron, *Radiology*, 2019, **291**, 273–284.
139 J. H. Ardenkjaer-Larsen, S. Bowen, J. R. Petersen, O. Rybalko, M. S. Vinding, M. Ullisch and N. C. Nielsen, *Magn. Reson. Med.*, 2019, **81**, 2184–2194.
140 T. Cheng, A. P. Gaunt, I. Marco-Rius, M. Gehrung, A. P. Chen, J. J. van der Klink and A. Comment, *NMR Biomed.*, 2020, **33**, e4264.
141 M. Baudin, B. Vuichoud, A. Bornet, G. Bodenhausen and S. Jannin, *J. Magn. Reson.*, 2018, **294**, 115–121.
142 L. L. Lumata, R. Martin, A. K. Jindal, Z. Kovacs, M. S. Conradi and M. E. Merritt, *MAGMA*, 2015, **28**, 195–205.
143 S. Jannin, A. Comment, F. Kurdzesau, J. A. Konter, P. Hautle, B. van den Brandt and J. J. van der Klink, *J. Chem. Phys.*, 2008, **128**, 241102.
144 M. L. Hirsch, N. Kalechofsky, A. Belzer, M. Rosay and J. G. Kempf, *J. Am. Chem. Soc.*, 2015, **137**, 8428–8434.
145 K. Golman, R. in 't Zandt and M. Thaning, *Proc. Natl. Acad. Sci. U. S. A.*, 2006, **103**, 11270–11275.
146 K. Golman, R. I. Zandt, M. Lerche, R. Pehrson and J. H. Ardenkjaer-Larsen, *Cancer Res.*, 2006, **66**, 10855–10860.
147 M. G. Vander Heiden, L. C. Cantley and C. B. Thompson, *Science*, 2009, **324**, 1029–1033.
148 B. T. Scroggins, M. Matsuo, A. O. White, K. Saito, J. P. Munasinghe, C. Sourbier, K. Yamamoto, V. Diaz, Y. Takakusagi, K. Ichikawa, J. B. Mitchell, M. C. Krishna and D. E. Citrin, *Clin. Cancer Res.*, 2018, **24**, 3137–3148.
149 A. Comment, *J. Magn. Reson.*, 2016, **264**, 39–48.
150 Y. Takakusagi, R. Kobayashi, K. Saito, S. Kishimoto, M. C. Krishna, R. Murugesan and K. I. Matsumoto, *Metabolites*, 2023, **13**, 69.
151 P. E. Z. Larson, *Hyperpolarized Carbon-13 Magnetic Resonance Imaging and Spectroscopy*, Academic Press, 2021.
152 Y. Kondo, H. Nonaka, Y. Takakusagi and S. Sando, *Angew. Chem., Int. Ed.*, 2021, **60**, 14779–14799.
153 C. Mu, D. E. Korenchan, S. Wang, D. M. Wilson and R. R. Flavell, *Mol. Imaging Biol.*, 2021, **23**, 323–334.
154 K. R. Keshari and D. M. Wilson, *Chem. Soc. Rev.*, 2014, **43**, 1627–1659.
155 P. R. Jensen, M. Karlsson, S. Meier, J. O. Duus and M. H. Lerche, *Chemistry*, 2009, **15**, 10010–10012.
156 P. Viswanath, G. Batsios, J. Mukherjee, A. M. Gillespie, P. E. Z. Larson, H. A. Luchman, J. J. Phillips, J. F. Costello, R. O. Pieper and S. M. Ronen, *Nat. Commun.*, 2021, **12**, 92.
157 R. Hata, H. Nonaka, Y. Takakusagi, K. Ichikawa and S. Sando, *Angew. Chem., Int. Ed.*, 2016, **55**, 1765–1768.
158 A. Radaelli, D. Ortiz, A. Michelotti, M. Roche, R. Hata, S. Sando, O. Bonny, R. Gruetter and H. A. I. Yoshihara, *ACS Sens.*, 2022, **7**, 2987–2994.
159 K. Yamamoto, A. Opina, D. Sail, B. Blackman, K. Saito, J. R. Brender, R. M. Malinowski, T. Seki, N. Oshima, D. R. Crooks, S. Kishimoto, Y. Saida, Y. Otowa, P. L. Choyke, J. H. Ardenkjaer-Larsen, J. B. Mitchell, W. M. Linehan, R. E. Swenson and M. C. Krishna, *Sci. Rep.*, 2021, **11**, 12155.
160 G. Batsios, C. Najac, P. Cao, P. Viswanath, E. Subramani, Y. Saito, A. M. Gillespie, H. A. I. Yoshihara, P. Larson, S. Sando and S. M. Ronen, *Sci. Rep.*, 2020, **10**, 6244.
161 T. Nishihara, H. A. Yoshihara, H. Nonaka, Y. Takakusagi, F. Hyodo, K. Ichikawa, E. Can, J. A. Bastiaansen, Y. Takado, A. Comment and S. Sando, *Angew. Chem., Int. Ed.*, 2016, **55**, 10626–10629.
162 Y. Saito, H. Yatabe, I. Tamura, Y. Kondo, R. Ishida, T. Seki, K. Hiraga, A. Eguchi, Y. Takakusagi, K. Saito, N. Oshima, H. Ishikita, K. Yamamoto, M. C. Krishna and S. Sando, *Sci. Adv.*, 2022, **8**, eabj2667.
163 R. Eskandari, N. Kim, A. Mamakhanyan, M. Saoi, G. Zhang, M. Berisaj, K. L. Granlund, A. J. Poot, J. Cross, C. B. Thompson and K. R. Keshari, *Proc. Natl. Acad. Sci. U. S. A.*, 2022, **119**, e2120595119.
164 Y. Imakura, H. Nonaka, Y. Takakusagi, K. Ichikawa, N. R. Maptue, A. M. Funk, C. Khemtong and S. Sando, *Chem. – Asian J.*, 2018, **13**, 280–283.
165 H. Nonaka, M. Hirano, Y. Imakura, Y. Takakusagi, K. Ichikawa and S. Sando, *Sci. Rep.*, 2017, **7**, 40104.
166 H. Nonaka, R. Hata, T. Doura, T. Nishihara, K. Kumagai, M. Akakabe, M. Tsuda, K. Ichikawa and S. Sando, *Nat. Commun.*, 2013, **4**, 2411.
167 A. Comment and M. E. Merritt, *Biochemistry*, 2014, **53**, 7333–7357.
168 J. Milani, B. Vuichoud, A. Bornet, P. Mieville, R. Mottier, S. Jannin and G. Bodenhausen, *Rev. Sci. Instrum.*, 2015, **86**, 024101.
169 K. Kouril, H. Kourilova, S. Bartram, M. H. Levitt and B. Meier, *Nat. Commun.*, 2019, **10**, 1733.
170 A. Capozzi, S. Patel, W. T. Wenckebach, M. Karlsson, M. H. Lerche and J. H. Ardenkjaer-Larsen, *J. Phys. Chem. Lett.*, 2019, **10**, 3420–3425.
171 L. Lumata, M. E. Merritt, C. R. Malloy, A. D. Sherry and Z. Kovacs, *J. Phys. Chem. A*, 2012, **116**, 5129–5138.
172 L. Lumata, M. E. Merritt and Z. Kovacs, *Phys. Chem. Chem. Phys.*, 2013, **15**, 7032–7035.
173 B. Lama, J. H. Collins, D. Downes, A. N. Smith and J. R. Long, *NMR Biomed.*, 2016, **29**, 226–231.

 This journal is © The Royal Society of Chemistry 2025

Open Access Article. Published on 28 Januarie 2025. Downloaded on 2026-01-31 2:57:56 nm.
This article is licensed under a Creative Commons Attribution-NonCommercial 3.0 Unported Licence.

174 A. P. Gaunt, J. S. Lewis, F. Hesse, T. Cheng, I. Marco-Rius, K. M. Brindle and A. Comment, *Angew. Chem., Int. Ed.*, 2022, **61**, e202112982.
175 A. Capozzi, S. Patel, C. P. Gunnarsson, I. Marco-Rius, A. Comment, M. Karlsson, M. H. Lerche, O. Ouari and J. H. Ardenkjaer-Larsen, *Angew. Chem., Int. Ed.*, 2019, **58**, 1334–1339.
176 T. El Darai, S. F. Cousin, Q. Stern, M. Ceillier, J. Kempf, D. Eshchenko, R. Melzi, M. Schnell, L. Gremillard, A. Bornet, J. Milani, B. Vuichoud, O. Cala, D. Montarnal and S. Jannin, *Nat. Commun.*, 2021, **12**, 4695.
177 D. Gajan, A. Bornet, B. Vuichoud, J. Milani, R. Melzi, H. A. van Kalkeren, L. Veyre, C. Thieuleux, M. P. Conley, W. R. Gruning, M. Schwarzwalder, A. Lesage, C. Coperet, G. Bodenhausen, L. Emsley and S. Jannin, *Proc. Natl. Acad. Sci. U. S. A.*, 2014, **111**, 14693–14697.
178 A. S. Kiryutin, B. A. Rodin, A. V. Yurkovskaya, K. L. Ivanov, D. Kurzbach, S. Jannin, D. Guarin, D. Abergel and G. Bodenhausen, *Phys. Chem. Chem. Phys.*, 2019, **21**, 13696–13705.
179 X. Ji, A. Bornet, B. Vuichoud, J. Milani, D. Gajan, A. J. Rossini, L. Emsley, G. Bodenhausen and S. Jannin, *Nat. Commun.*, 2017, **8**, 13975.
180 R. L. Hesketh and K. M. Brindle, *Curr. Opin. Chem. Biol.*, 2018, **45**, 187–194.
181 T. B. Rodrigues, E. M. Serrao, B. W. Kennedy, D. E. Hu, M. I. Kettunen and K. M. Brindle, *Nat. Med.*, 2014, **20**, 93–97.
182 S. E. Day, M. I. Kettunen, F. A. Gallagher, D. E. Hu, M. Lerche, J. Wolber, K. Golman, J. H. Ardenkjaer-Larsen and K. M. Brindle, *Nat. Med.*, 2007, **13**, 1382–1387.
183 K. R. Keshari, J. Kurhanewicz, J. M. Macdonald and D. M. Wilson, *Analyst*, 2012, **137**, 3427–3429.
184 M. H. Lerche, S. Meier, P. R. Jensen, H. Baumann, B. O. Petersen, M. Karlsson, J. O. Duus and J. H. Ardenkjaer-Larsen, *J. Magn. Reson.*, 2010, **203**, 52–56.
185 P. Nikolaou, B. M. Goodson and E. Y. Chekmenev, *Chemistry*, 2015, **21**, 3156–3166.
186 M. Iinuma, Y. Takahashi, I. Shaké, M. Oda, A. Masaike, T. Yabuzaki and H. M. Shimizu, *Phys. Rev. Lett.*, 2000, **84**, 171–174.
187 P. Bachert, H. Brunner, K. H. Hausser and J. P. Colpa, *Chem. Phys.*, 1984, **91**, 435–447.
188 A. Kagawa, M. Negoro, R. Ohba, N. Ichijo, K. Takamine, Y. Nakamura, T. Murata, Y. Morita and M. Kitagawa, *J. Phys. Chem. A*, 2018, **122**, 9670–9675.
189 K. Tateishi, M. Negoro, S. Nishida, A. Kagawa, Y. Morita and M. Kitagawa, *Proc. Natl. Acad. Sci. U. S. A.*, 2014, **111**, 7527–7530.
190 M. Negoro, A. Kagawa, K. Tateishi, Y. Tanaka, T. Yuasa, K. Takahashi and M. Kitagawa, *J. Phys. Chem. A*, 2018, **122**, 4294–4297.
191 A. Kagawa, K. Miyanishi, N. Ichijo, M. Negoro, Y. Nakamura, H. Enozawa, T. Murata, Y. Morita and M. Kitagawa, *J. Magn. Reson.*, 2019, **309**, 106623.
192 T. Hamachi, K. Nishimura, H. Kouno, Y. Kawashima, K. Tateishi, T. Uesaka, N. Kimizuka and N. Yanai, *J. Phys. Chem. Lett.*, 2021, **12**, 2645–2650.
193 K. Nishimura, H. Kouno, Y. Kawashima, K. Orihashi, S. Fujiwara, K. Tateishi, T. Uesaka, N. Kimizuka and N. Yanai, *Chem. Commun.*, 2020, **56**, 7217–7232.
194 H. Sato, K. Miyanishi, M. Negoro, A. Kagawa, Y. Nishiyama, S. Horike, K. Nakamura and M. Inukai, *J. Phys. Chem. Lett.*, 2023, **14**, 4560–4564.
195 S. Fujiwara, N. Matsumoto, K. Nishimura, N. Kimizuka, K. Tateishi, T. Uesaka and N. Yanai, *Angew. Chem., Int. Ed.*, 2022, **61**, e202115792.
196 K. Tateishi, M. Negoro, A. Kagawa and M. Kitagawa, *Angew. Chem., Int. Ed.*, 2013, **52**, 13307–13310.
197 Y. Kawashima, T. Hamachi, A. Yamauchi, K. Nishimura, Y. Nakashima, S. Fujiwara, N. Kimizuka, T. Ryu, T. Tamura, M. Saigo, K. Onda, S. Sato, Y. Kobori, K. Tateishi, T. Uesaka, G. Watanabe, K. Miyata and N. Yanai, *Nat. Commun.*, 2023, **14**, 1056.
198 K. Miyanishi, T. Sugiki, T. Matsui, R. Ozawa, Y. Hatanaka, H. Enozawa, Y. Nakamura, T. Murata, A. Kagawa, Y. Morita, T. Fujiwara, M. Kitagawa and M. Negoro, *J. Phys. Chem. Lett.*, 2023, **14**, 6241–6247.
199 A. Eldirdiri, A. Clemmensen, S. Bowen, A. Kjaer and J. H. Ardenkjaer-Larsen, *NMR Biomed.*, 2017, **30**, e3803.
200 D. M. Wilson, K. R. Keshari, P. E. Larson, A. P. Chen, S. Hu, M. Van Criekinge, R. Bok, S. J. Nelson, J. M. Macdonald, D. B. Vigneron and J. Kurhanewicz, *J. Magn. Reson.*, 2010, **205**, 141–147.
201 H. Qin, V. Zhang, R. A. Bok, R. D. Santos, J. A. Cunha, I. C. Hsu, J. D. Santos Bs, J. E. Lee, S. Sukumar, P. E. Z. Larson, D. B. Vigneron, D. M. Wilson, R. Sriram and J. Kurhanewicz, *Int. J. Radiat. Oncol., Biol., Phys.*, 2020, **107**, 887–896.
202 H. Gutte, A. E. Hansen, M. M. Larsen, S. Rahbek, S. T. Henriksen, H. H. Johannesen, J. Ardenkjaer-Larsen, A. T. Kristensen, L. Hojgaard and A. Kjaer, *J. Nucl. Med.*, 2015, **56**, 1786–1792.
203 Z. M. Bhujwalla, S. Kakkad, Z. Chen, J. Jin, S. Hapuarachchige, D. Artemov and M. F. Penet, *J. Magn. Reson.*, 2018, **291**, 141–151.
204 C. Hilty, D. Kurzbach and L. Frydman, *Nat. Protoc.*, 2022, **17**, 1621–1657.
205 K. K. Frederick, V. K. Michaelis, B. Corzilius, T. C. Ong, A. C. Jacavone, R. G. Griffin and S. Lindquist, *Cell*, 2015, **163**, 620–628.
206 G. Angelovski, B. J. Tickner and G. Wang, *Nat. Chem.*, 2023, **15**, 755–763.
207 M. I. Franco, L. Turin, A. Mershin and E. M. Skoulakis, *Proc. Natl. Acad. Sci. U. S. A.*, 2011, **108**, 3797–3802.
208 E. Block, S. Jang, H. Matsunami, S. Sekharan, B. Dethier, M. Z. Ertem, S. Gundala, Y. Pan, S. Li, Z. Li, S. N. Lodge, M. Ozbil, H. Jiang, S. F. Penalba, V. S. Batista and H. Zhuang, *Proc. Natl. Acad. Sci. U. S. A.*, 2015, **112**, E2766–E2774.
209 R. D. Hoehn, D. E. Nichols, H. Heven and S. Kais, *Front. Phys.*, 2018, **6**, 25.
210 S. Johnsen and K. J. Lohmann, *Nat. Rev. Neurosci.*, 2005, **6**, 703–712.

Open Access Article. Published on 28 Januarie 2025. Downloaded on 2026-01-31 2:57:56 nm.
This article is licensed under a Creative Commons Attribution-NonCommercial 3.0 Unported Licence.

211 H. Mouritsen and T. Ritz, *Curr. Opin. Neurobiol.*, 2005, **15**, 406–414.
212 T. Ritz, S. Adem and K. Schulten, *Biophys. J.*, 2000, **78**, 707–718.
213 J. Xu, L. E. Jarocha, T. Zollitsch, M. Konowalczyk, K. B. Henbest, S. Richert, M. J. Golesworthy, J. Schmidt, V. Déjean, D. J. C. Sowood, M. Bassetto, J. Luo, J. R. Walton, J. Fleming, Y. Wei, T. L. Pitcher, G. Moise, M. Herrmann, H. Yin, H. Wu, R. Bartölke, S. J. Käsehagen, S. Horst, G. Dautaj, P. D. F. Murton, A. S. Gehrckens, Y. Chelliah, J. S. Takahashi, K.-W. Koch, S. Weber, I. A. Solov'yov, C. Xie, S. R. Mackenzie, C. R. Timmel, H. Mouritsen and P. J. Hore, *Nature*, 2021, **594**, 535–540.
214 T. Hochstoeger, T. Al Said, D. Maestre, F. Walter, A. Vilceanu, M. Pedron, T. D. Cushion, W. Snider, S. Nimpf, G. C. Nordmann, L. Landler, N. Edelman, L. Kruppa, G. Dürnberger, K. Mechtler, S. Schuechner, E. Ogris, E. P. Malkemper, S. Weber, E. Schleicher and D. A. Keays, *Sci. Adv.*, 2020, **6**, eabb9110.
215 H. Mitsui, T. Maeda, C. Yamaguchi, Y. Tsuji, R. Watari, Y. Kubo, K. Okano and T. Okano, *Biochemistry*, 2015, **54**, 1908–1917.
216 H. Otsuka, H. Mitsui, K. Miura, K. Okano, Y. Imamoto and T. Okano, *Biochemistry*, 2020, **59**, 3615–3625.
217 R. Watari, C. Yamaguchi, W. Zemba, Y. Kubo, K. Okano and T. Okano, *J. Biol. Chem.*, 2012, **287**, 42634–42641.
218 M. Liedvogel, K. Maeda, K. Henbest, E. Schleicher, T. Simon, C. R. Timmel, P. J. Hore and H. Mouritsen, *PLoS One*, 2007, **2**, e1106.
219 R. J. Gegear, L. E. Foley, A. Casselman and S. M. Reppert, *Nature*, 2010, **463**, 804–807.
220 D. M. W. Sheppard, J. Li, K. B. Henbest, S. R. T. Neil, K. Maeda, J. Storey, E. Schleicher, T. Biskup, R. Rodriguez, S. Weber, P. J. Hore, C. R. Timmel and S. R. Mackenzie, *Sci. Rep.*, 2017, **7**, 42228.
221 O. Bazalova, M. Kvicalova, T. Valkova, P. Slaby, P. Bartos, R. Netusil, K. Tomanova, P. Braeunig, H.-J. Lee, I. Sauman, M. Damulewicz, J. Provaznik, R. Pokorny, D. Dolezel and M. Vacha, *Proc. Natl. Acad. Sci. U. S. A.*, 2016, **113**, 1660–1665.
222 H. G. Hiscock, S. Worster, D. R. Kattnig, C. Steers, Y. Jin, D. E. Manolopoulos, H. Mouritsen and P. J. Hore, *Proc. Natl. Acad. Sci. U. S. A.*, 2016, **113**, 4634–4639.
223 K. Maeda, J. G. Storey, P. A. Liddell, D. Gust, P. J. Hore, C. J. Wedge and C. R. Timmel, *Phys. Chem. Chem. Phys.*, 2015, **17**, 3550–3559.
224 M. Pooam, L.-D. Arthaut, D. Burdick, J. Link, C. F. Martino and M. Ahmad, *Planta*, 2019, **249**, 319–332.
225 K. Maeda, A. J. Robinson, K. B. Henbest, H. J. Hogben, T. Biskup, M. Ahmad, E. Schleicher, S. Weber, C. R. Timmel and P. J. Hore, *Proc. Natl. Acad. Sci. U. S. A.*, 2012, **109**, 4774–4779.
226 C. T. Rodgers and P. J. Hore, *Proc. Natl. Acad. Sci. U. S. A.*, 2009, **106**, 353–360.
227 B. D. Zoltowski, Y. Chelliah, A. Wickramaratne, L. Jarocha, N. Karki, W. Xu, H. Mouritsen, P. J. Hore, R. E. Hibbs, C. B. Green and J. S. Takahashi, *Proc. Natl. Acad. Sci. U. S. A.*, 2019, **116**, 19449–19457.
228 B. Brocklehurst, *Chem. Soc. Rev.*, 2002, **31**, 301–311.
229 U. E. Steiner and T. Ulrich, *Chem. Rev.*, 1989, **89**, 51–147.
230 C. Kerpal, S. Richert, J. G. Storey, S. Pillai, P. A. Liddell, D. Gust, S. R. Mackenzie, P. J. Hore and C. R. Timmel, *Nat. Commun.*, 2019, **10**, 3707.
231 F. Cintolesi, T. Ritz, C. W. M. Kay, C. R. Timmel and P. J. Hore, *Chem. Phys.*, 2003, **294**, 385–399.
232 P. J. Hore and H. Mouritsen, *Annu. Rev. Biophys.*, 2016, **45**, 299–344.
233 K. Maeda, K. B. Henbest, F. Cintolesi, I. Kuprov, C. T. Rodgers, P. A. Liddell, D. Gust, C. R. Timmel and P. J. Hore, *Nature*, 2008, **453**, 387–390.
234 H. J. Hogben, O. Efimova, N. Wagner-Rundell, C. R. Timmel and P. J. Hore, *Chem. Phys. Lett.*, 2009, **480**, 118–122.
235 S. Arai, R. Shimizu, M. Adachi and M. Hirai, *Protein Sci.*, 2022, **31**, e4313.
236 S. Qin, H. Yin, C. Yang, Y. Dou, Z. Liu, P. Zhang, H. Yu, Y. Huang, J. Feng, J. Hao, J. Hao, L. Deng, X. Yan, X. Dong, Z. Zhao, T. Jiang, H.-W. Wang, S.-J. Luo and C. Xie, *Nat. Mater.*, 2016, **15**, 217–226.
237 H. Wu, A. Scholten, A. Einwich, H. Mouritsen and K.-W. Koch, *Sci. Rep.*, 2020, **10**, 7364.
238 C. Xie, *The Innovation*, 2022, **3**, 100229.
239 H. Xie, A. Lyratzakis, R. Khera, M. Koutantou, S. Welsch, H. Michel and G. Tsiotis, *Proc. Natl. Acad. Sci. U. S. A.*, 2023, **120**, e2216734120.
240 D. E. Tronrud, J. Wen, L. Gay and R. E. Blankenship, *Photosynth. Res.*, 2009, **100**, 79–87.
241 I. A. Solov'yov and K. Schulten, *Biophys. J.*, 2009, **96**, 4804–4813.
242 C. Nießner, S. Denzau, K. Stapput, M. Ahmad, L. Peichl, W. Wiltschko and R. Wiltschko, *J. R. Soc., Interface*, 2013, **10**, 20130638.
243 C. Nießner, S. Denzau, J. C. Gross, L. Peichl, H.-J. Bischof, G. Fleissner, W. Wiltschko and R. Wiltschko, *PLoS One*, 2011, **6**, e20091.
244 P. Bolte, A. Einwich, P. K. Seth, R. Chetverikova, D. Heyers, I. Wojahn, U. Janssen-Bienhold, R. Feederle, P. Hore, K. Dedek and H. Mouritsen, *Ethology Ecology Evolution*, 2021, **33**, 248–272.
245 P. Müller and M. Ahmad, *J. Biol. Chem.*, 2011, **286**, 21033–21040.
246 C. Nießner, S. Denzau, L. Peichl, W. Wiltschko and R. Wiltschko, *J. Exp. Biol.*, 2014, **217**, 4221–4224.
247 C. Nießner, S. Denzau, L. Peichl, W. Wiltschko and R. Wiltschko, *J. Comp. Physiol., A*, 2018, **204**, 977–984.
248 T. C. Player and P. J. Hore, *J. Chem. Phys.*, 2019, **151**, 225101.
249 R. Wiltschko, M. Ahmad, C. Nießner, D. Gehring and W. Wiltschko, *J. R. Soc., Interface*, 2016, **13**, 20151010.
250 R. J. Kutta, N. Archipowa, L. O. Johannissen, A. R. Jones and N. S. Scrutton, *Sci. Rep.*, 2017, **7**, 44906.
251 R. J. Gegear, A. Casselman, S. Waddell and S. M. Reppert, *Nature*, 2008, **454**, 1014–1018.
252 A. A. Bradlaugh, G. Fedele, A. L. Munro, C. N. Hansen, J. M. Hares, S. Patel, C. P. Kyriacou, A. R. Jones, E. Rosato and R. A. Baines, *Nature*, 2023, **615**, 111–116.

 This journal is © The Royal Society of Chemistry 2025

Open Access Article. Published on 28 Januarie 2025. Downloaded on 2026-01-31 2:57:56 nm.
This article is licensed under a Creative Commons Attribution-NonCommercial 3.0 Unported Licence.

253 E. W. Evans, C. A. Dodson, K. Maeda, T. Biskup, C. J. Wedge and C. R. Timmel, *Interface Focus.*, 2013, **3**, 20130037.
254 N. Ikeya and J. R. Woodward, *Proc. Natl. Acad. Sci. U. S. A.*, 2021, **118**, e2018043118.
255 D. Shevela, J. F. Kern, G. Govindjee and J. Messinger, *Photosynth. Res.*, 2023, **156**, 279–307.
256 T. Mirkovic, E. E. Ostroumov, J. M. Anna, R. Van Grondelle, G. Govindjee and G. D. Scholes, *Chem. Rev.*, 2017, **117**, 249–293.
257 M. L. Groot, J. P. Dekker, R. Van Grondelle, F. T. H. Den Hartog and S. Völker, *J. Phys. Chem.*, 1996, **100**, 11488–11495.
258 E. Wientjes, H. Van Amerongen and R. Croce, *J. Phys. Chem. B*, 2013, **117**, 11200–11208.
259 M. Mamedov, G. Govindjee, V. Nadtochenko and A. Semenov, *Photosynth. Res.*, 2015, **125**, 51–63.
260 E. Romero, I. H. M. Van Stokkum, V. I. Novoderezhkin, J. P. Dekker and R. Van Grondelle, *Biochemistry*, 2010, **49**, 4300–4307.
261 W. Lubitz, M. Chrysina and N. Cox, *Photosynth. Res.*, 2019, **142**, 105–125.
262 Y. Umena, K. Kawakami, J.-R. Shen and N. Kamiya, *Nature*, 2011, **473**, 55–60.
263 A. Galstyan, A. Robertazzi and E. W. Knapp, *J. Am. Chem. Soc.*, 2012, **134**, 7442–7449.
264 S. Luber, I. Rivalta, Y. Umena, K. Kawakami, J.-R. Shen, N. Kamiya, G. W. Brudvig and V. S. Batista, *Biochemistry*, 2011, **50**, 6308–6311.
265 M. Suga, F. Akita, K. Hirata, G. Ueno, H. Murakami, Y. Nakajima, T. Shimizu, K. Yamashita, M. Yamamoto, H. Ago and J.-R. Shen, *Nature*, 2015, **517**, 99–103.
266 A. Bhowmick, R. Hussein, I. Bogacz, P. S. Simon, M. Ibrahim, R. Chatterjee, M. D. Doyle, M. H. Cheah, T. Fransson, P. Chernev, I.-S. Kim, H. Makita, M. Dasgupta, C. J. Kaminsky, M. Zhang, J. Gätcke, S. Haupt, I. I. Nangca, S. M. Keable, A. O. Aydin, K. Tono, S. Owada, L. B. Gee, F. D. Fuller, A. Batyuk, R. Alonso-Mori, J. M. Holton, D. W. Paley, N. W. Moriarty, F. Mamedov, P. D. Adams, A. S. Brewster, H. Dobbek, N. K. Sauter, U. Bergmann, A. Zouni, J. Messinger, J. Kern, J. Yano and V. K. Yachandra, *Nature*, 2023, **617**, 629–636.
267 M. Suga, F. Akita, K. Yamashita, Y. Nakajima, G. Ueno, H. Li, T. Yamane, K. Hirata, Y. Umena, S. Yonekura, L.-J. Yu, H. Murakami, T. Nomura, T. Kimura, M. Kubo, S. Baba, T. Kumasaka, K. Tono, M. Yabashi, H. Isobe, K. Yamaguchi, M. Yamamoto, H. Ago and J.-R. Shen, *Science*, 2019, **366**, 334–338.
268 V. Krewald, M. Retegan, N. Cox, J. Messinger, W. Lubitz, S. DeBeer, F. Neese and D. A. Pantazis, *Chem. Sci.*, 2015, **6**, 1676–1695.
269 M. Şener, J. Strümpfer, J. Hsin, D. Chandler, S. Scheuring, C. N. Hunter and K. Schulten, *ChemPhysChem*, 2011, **12**, 518–531.
270 A. M. Van Oijen, M. Ketelaars, J. Köhler, T. J. Aartsma and J. Schmidt, *Science*, 1999, **285**, 400–402.
271 A. Chenu and G. D. Scholes, *Annu. Rev. Phys. Chem.*, 2015, **66**, 69–96.
272 A. Ishizaki and G. R. Fleming, *Annu. Rev. Condens. Matter Phys.*, 2012, **3**, 333–361.
273 G. S. Engel, T. R. Calhoun, E. L. Read, T.-K. Ahn, T. Mančal, Y.-C. Cheng, R. E. Blankenship and G. R. Fleming, *Nature*, 2007, **446**, 782–786.
274 S. I. E. Vulto, M. A. De Baat, S. Neerken, F. R. Nowak, H. Van Amerongen, J. Amesz and T. J. Aartsma, *J. Phys. Chem. B*, 1999, **103**, 8153–8161.
275 J. Cao, R. J. Cogdell, D. F. Coker, H.-G. Duan, J. Hauer, U. Kleinekathöfer, T. L. C. Jansen, T. Mančal, R. J. D. Miller, J. P. Ogilvie, V. I. Prokhorenko, T. Renger, H.-S. Tan, R. Tempelaar, M. Thorwart, E. Thyrhaug, S. Westenhoff and D. Zigmantas, *Sci. Adv.*, 2020, **6**, eaaz4888.
276 F. Fassioli, R. Dinshaw, P. C. Arpin and G. D. Scholes, *J. R. Soc., Interface*, 2014, **11**, 20130901.
277 N. Lambert, Y.-N. Chen, Y.-C. Cheng, C.-M. Li, G.-Y. Chen and F. Nori, *Nat. Phys.*, 2013, **9**, 10–18.
278 S. Roeding and T. Brixner, Coherent two-dimensional electronic mass spectrometry, *Nat. Commun.*, 2018, **9**, 2519.
279 E. Collini, J 2D Electronic Spectroscopic Techniques for Quantum Technology Applications, *J. Phys. Chem. C*, 2021, **125**, 13096–13108.
280 N.-U. Frigaard and D. A. Bryant, in *Complex Intracellular Structures in Prokaryotes*, ed. J. M. Shively, Springer Berlin Heidelberg, Berlin, Heidelberg, 2006, vol. **2**, pp. 79–114.
281 J. Adolphs and T. Renger, *Biophys. J.*, 2006, **91**, 2778–2797.
282 J. Moix, J. Wu, P. Huo, D. Coker and J. Cao, *J. Phys. Chem. Lett.*, 2011, **2**, 3045–3052.
283 J.-H. Chen, H. Wu, C. Xu, X.-C. Liu, Z. Huang, S. Chang, W. Wang, G. Han, T. Kuang, J.-R. Shen and X. Zhang, *Science*, 2020, **370**, eabb6350.
284 G. Panitchayangkoon, D. V. Voronine, D. Abramavicius, J. R. Caram, N. H. C. Lewis, S. Mukamel and G. S. Engel, *Proc. Natl. Acad. Sci. U. S. A.*, 2011, **108**, 20908–20912.
285 H. Lee, Y.-C. Cheng and G. R. Fleming, *Science*, 2007, **316**, 1462–1465.
286 B. S. Rolczynski, H. Zheng, V. P. Singh, P. Navotnaya, A. R. Ginzburg, J. R. Caram, K. Ashraf, A. T. Gardiner, S.-H. Yeh, S. Kais, R. J. Cogdell and G. S. Engel, *Chem*, 2018, **4**, 138–149.
287 J. S. Higgins, L. T. Lloyd, S. H. Sohail, M. A. Allodi, J. P. Otto, R. G. Saer, R. E. Wood, S. C. Massey, P.-C. Ting, R. E. Blankenship and G. S. Engel, *Proc. Natl. Acad. Sci. U. S. A.*, 2021, **118**, e2018240118.
288 L. Wang, M. A. Allodi and G. S. Engel, *Nat. Rev. Chem.*, 2019, **3**, 477–490.
289 H.-G. Duan, V. I. Prokhorenko, R. J. Cogdell, K. Ashraf, A. L. Stevens, M. Thorwart and R. J. D. Miller, *Proc. Natl. Acad. Sci. U. S. A.*, 2017, **114**, 8493–8498.
290 E. Thyrhaug, R. Tempelaar, M. J. P. Alcocer, K. Žídek, D. Bína, J. Knoester, T. L. C. Jansen and D. Zigmantas, *Nat. Chem.*, 2018, **10**, 780–786.
291 S. Niwa, L.-J. Yu, K. Takeda, Y. Hirano, T. Kawakami, Z.-Y. Wang-Otomo and K. Miki, *Nature*, 2014, **508**, 228–232.
292 X. Qin, M. Suga, T. Kuang and J.-R. Shen, *Science*, 2015, **348**, 989–995.

Open Access Article. Published on 28 Januarie 2025. Downloaded on 2026-01-31 2:57:56 nm.
This article is licensed under a Creative Commons Attribution-NonCommercial 3.0 Unported Licence.

293 X. Wei, X. Su, P. Cao, X. Liu, W. Chang, M. Li, X. Zhang and Z. Liu, *Nature*, 2016, **534**, 69–74.
294 K. Kato, N. Miyazaki, T. Hamaguchi, Y. Nakajima, F. Akita, K. Yonekura and J.-R. Shen, *Commun. Biol.*, 2021, **4**, 382.
295 E. Schrödinger, *What Is Life? The Physical Aspect of the Living Cell*, Cambridge University Press, Cambridge, 1944.
296 M. P. Meyer, D. R. Tomchick and J. P. Klinman, *Proc. Natl. Acad. Sci. U. S. A.*, 2008, **105**, 1146–1151.
297 M. Horitani, A. R. Offenbacher, C. A. M. Carr, T. Yu, V. Hoeke, G. E. Cutsail III, S. H. Schiffer, J. P. Klinman and B. M. Hoffman, *J. Am. Chem. Soc.*, 2017, **139**(5), 1984–1997.
298 A. R. Offenbacher, A. Sharma, P. E. Doan, J. P. Klinman and B. M. Hoffman, *Biochemistry*, 2020, **59**(7), 901–910.
299 Z.-X. Liang, T. Lee, K. A. Resing, N. G. Ahn and J. P. Klinman, *Proc. Natl. Acad. Sci. U. S. A.*, 2004, **101**, 9556.
300 A. R. Offenbacher, S. Hu, E. M. Poss, C. A. M. Carr, A. D. Scouras, D. M. Prigozhin, A. T. Iavarone, A. Palla, T. Alber, J. S. Fraser and J. P. Klinman, *ACS Cent. Sci.*, 2017, **3**, 570–579.
301 J. Zhang, J. L. Balsbaugh, S. Gao, N. G. Ahn and J. P. Klinman, *Proc. Natl. Acad. Sci. U. S. A.*, 2020, **117**, 10797.
302 S. Gao, E. J. Thompson, S. L. Barrow, W. Zhang, A. T. Iavarone and J. P. Klinman, *J. Am. Chem. Soc.*, 2020, **142**, 19936–19949.
303 E. J. Thompson, A. Paul, A. T. Iavarone and J. P. Klinman, *J. Am. Chem. Soc.*, 2021, **143**, 785–797.
304 E. J. Thompson, A. Paul, A. T. Iavarone and J. P. Klinman, *Proc. Natl. Acad. Sci. U. S. A.*, 2023, **120**, e2211630120.
305 J. D. Watson and F. H. C. Crick, The structure of DNA, *Cold Spring Harbor Symp. Quant. Biol.*, 1953, **18**, 123–131.
306 P. O. Löwdin, *Rev. Mod. Phys.*, 1963, **35**, 724–732.
307 A. B. Loveland, G. Demo, N. Grigorieff and A. A. Korostelev, *Nature*, 2017, **546**, 113–117.
308 I. J. Kimsey, E. S. Szymanski, W. J. Zahurancik, A. Shakya, Y. Xue, C. C. Chu, B. Sathyamoorthy, Z. Suo and H. M. Al-Hashimi, *Nature*, 2018, **554**, 195–201.
309 C. Tomasetti, L. Li and B. Vogelstein, *Science*, 2017, **355**, 1330–1334.
310 L. Slocombe, J. S. Al-Khalilib and M. Sacchi, *Phys. Chem. Chem. Phys.*, 2021, **23**, 4141.
311 O. O. Brovarets and D. M. Hovorun, *J. Biomol. Struct. Dyn.*, 2019, **37**, 1880–1907.
312 A. Gheorghiu, P. Coveney and A. Arabi, *Interface Focus*, 2020, **10**, 20190120.
313 L. Slocombe, M. Sacchi and J. Al-Khalili, *Commun. Phys.*, 2022, **5**, 109.
314 M. Maestre-Reyna, P.-H. Wang, E. Nango, Y. Hosokawa, M. Saft, A. Furrer, C.-H. Yang, E. P. G. N. Putu, W.-J. Wu, H.-J. Emmerich, N. Caramello, S. Franz-Badur, C. Yang, S. Engilberge, M. Wranik, H. L. Glover, T. Weinert, H.-Y. Wu, C.-C. Lee, W.-C. Huang, K.-F. Huang, Y.-K. Chang, J.-H. Liao, J.-H. Weng, W. Gad, C.-W. Chang, A. H. Pang, K.-C. Yang, W.-T. Lin, Y.-C. Chang, D. Gashi, E. Beale, D. Ozerov, K. Nass, G. Knopp, P. J. M. Johnson, C. Cirelli, C. Milne, C. Bacellar, M. Sugahara, S. Owada, Y. Joti, A. Yamashita, R. Tanaka, T. Tanaka, F. Luo, K. Tono, W. Zarzycka, P. Müller, M. A. Alahmad, F. Bezold, V. Fuchs, P. Gnau, S. Kiontke, L. Korf, V. Reithofer, C. J. Rosner, E. M. Seiler, M. Watad, L. Werel, R. Spadaccini, J. Yamamoto, S. Iwata, D. Zhong, J. Standfuss, A. Royant, Y. Bessho, L.-O. Essen and M.-D. Tsai, *Science*, 2023, **382**, 1014.
315 M. Tsubouchi, N. Ishii, Y. Kagotani, R. Shimizu, T. Fujita, M. Adachi and R. Itakura, *Opt. Express*, 2023, **31**, 6890–6906.

 This journal is © The Royal Society of Chemistry 2025